Student thesis series INES nr 306

Modelling methane emissions from Arctic tundra wetlands: effects of fractional wetland maps

Zhanzhang Cai

2014
Department of Earth and Ecosystem Sciences
Physical Geography and Ecosystems Analysis
Lund University
Sölvegatan 12
S-223 62 Lund
Sweden

Zhanzhang Cai (2014). Modelling methane emissions from Arctic tundra wetlands: effects of fractional wetland maps
Master degree thesis, 30 credits in Physical Geography and Ecosystem Analysis
Department of Physical Geography and Ecosystems Science, Lund University

Modelling methane emissions from Arctic tundra wetlands: effects of fractional wetland maps

Zhanzhang Cai

Master thesis, 30 credits, in Physical Geography and Ecosystem Analysis

Supervisor 1: PhD, Paul Miller

Department of Physical Geography and Ecosystems Science, Lund University

Supervisor 2: PhD Student Wenxin Zhang

Department of Physical Geography and Ecosystems Science, Lund University

Abstract

The Arctic tundra has been considered as one of the most sensitive areas to global climate change. One impact of global warming is that permafrost thawing could result in more waterlogged and anaerobic conditions, and consequently an increasing release of methane (CH_4) to the atmosphere. These potential CH_4 emissions can further amplify global warming. Therefore, it is important to assess the quantity of CH_4 emissions from Arctic tundra wetlands and their sensitivity to climate change. Process-based CH_4 modelling is commonly used to estimate CH_4 emissions using single-source fractional wetland maps; however, it is not clear how the difference among multisource of fractional wetland maps affects CH_4 estimations. In this study LPJ-GUESS WHyMe was applied to simulate CH_4 emissions of Arctic tundra between 1961 and 2009 by using multisource fractional wetland maps, and their quantitative and qualitative differences in estimating CH_4 emissions from these fractional wetland maps was compared. Parameter sensitivity tests and a parameter optimization for the model were performed before the model was applied to Arctic tundra. The CH_4/CO_2 production ratio under anaerobic conditions (CH_4/CO_2) and fraction of available oxygen used for methane oxidation (f_{oxid}) were identified as the most important model parameters in estimating total CH_4 fluxes of Arctic tundra in the period 1961-2009. The regional simulation using multisource fractional wetland maps showed that the uncertainties of CH_4 emissions in Arctic tundra caused by fractional wetland maps were larger than that due to parameter uncertainty. However, the temporal variability of CH_4 emissions in Arctic tundra is not significantly different when using different fractional wetland maps. For different transport pathways of CH_4 emissions, diffusion was determined as the dominant pathway for methane transport from wetland to the atmosphere in Arctic tundra. CH_4 fluxes in Arctic tundra are more sensitive to soil temperature at 25 cm if the water table position is above the soil surface.

Keywords: LPJ-GUESS, Biogeochemical modelling, Methane emissions, Arctic tundra, Fractional wetland maps, Sensitivity test, Parameter optimization

Acknowledgements

First of all, I would like to give my full gratitude to Dr. Paul Miller and Ph.D. student, Wenxin Zhang, for their guidance, patience, and wisdom to help me finish this thesis. Secondly, I would also like to acknowledge Minchao Wu, Jing Tang, and Zhendong Wu for discussion of the model setup and improvements. The comments and suggestions by Professor Ben Smith, Dr. Margareta Johansson and master student Joel Forsmoo have greatly improved this thesis. Lastly, I would like to thank my parents and my friend Xiyin for all their love and encouragement.

Table of Contents

1 Introduction

Methane (CH_4) is the second most important long-lived greenhouse gas contributing to global radiative forcing. The global abundance of atmospheric CH_4 (1803 ± 2 ppb in 2011) is much lower than atmospheric CO_2 (390.5 ± 0.2 ppm in 2011). However, the radiative efficiency (W m^{-2} ppb^{-1}) of CH_4 is about 26 times that of CO_2 on a 100-year basis (Hartmann et al. 2013). Consequently, CH_4 (0.48 ± 0.05 W m^{-2} in 2011) produced about 17% of the total radiative forcing (2.83 ± 0.03 W m^{-2} in 2011) compared to CO_2 (1.82 ± 0.19 W m^{-2} in 2011), which produced about 64% of the total radiative forcing. (Myhre et al. 2013).

Reviewing the historical record of the global atmospheric concentrations of CH_4 since 1961, the first three decades have been considered as periods of increasing atmospheric CH_4, but its growth rate declined in the following decade (1990s) (Dlugokencky et al. 2011). The atmospheric concentration of CH_4 was then nearly constant from 1999 to 2006; followed by a rise again since 2007 (Kirschke et al. 2013). The causes for the recent variations of the atmospheric concentration of CH_4 are still poorly understood (Kirschke et al. 2013). Thus, it is worth to further study how the single most dominant natural CH_4 source to the global flux and inter-annual variability, which is CH_4 emission from wetlands and amounted to 177 to 284 Tg yr^{-1} during the years 2000 to 2009 (Hodson et al. 2011; Ringeval et al. 2011; Spahni et al. 2011), contributed to the variations of the atmospheric CH_4 concentration since 1961.

Warming of high latitudes and polar amplification is common to most climate model simulations (Ciais et al. 2013). One expected impact of global warming is that enhanced permafrost thawing could provide more water-logged and anaerobic conditions, leading to 7 to 17 Pg C lost, partly in the form of CH_4, over the 21st century (Zhuang et al. 2006). The Arctic tundra contains a widely distribution of continuous and discontinuous permafrost. Between 1990 and 2006, the Arctic tundra was a source of CH_4 to the atmosphere (19 Tg C yr^{-1}; uncertainty between sources of 8 and 29 TgC yr^{-1}), and the emissions of CH_4 from Arctic tundra was increasing continuously during this period (McGuire et al. 2012).

In order to quantitatively simulate past, present, and future CH_4 emissions from wetlands, a number of process-based methane models have been developed (e.g. Cao et al. 1996; Walter & Heimann 2000; Zhuang et al. 2004). Wania (2007) reviewed these models and found that very few models included important dynamic interactions between hydrology, soil temperature, vegetation and methane processes. In this regard, Wania et al. (2010) described

and evaluated a process-based model, LPJ-WHyMe (LPJ Wetland Hydrology and Methane), which was built on the LPJ-DGVM framework and took the interactions mentioned above into account.

In this thesis, the Wania et al. (2010) methane model to estimate CH_4 emissions from the Arctic tundra region was applied. Instead of LPJ-DGVM, however, the methane model will be run as a module within an individual-based dynamic vegetation model LPJ-GUESS (the Lund-Potsdam-Jena General Ecosystem Simulator) , which shares the mechanistic formulations of biophysics, phenology, plant physiology and biogeochemistry with LPJ-DGVM, but also adopts the formulation of gap model to explicitly simulate resource competition and canopy structure among cohort-averaged plant species (Smith et al. 2001). The model, LPJ-GUESS WHyMe, is used to estimate CH_4 emissions from wetlands within Arctic tundra defined by McGuire et al. (2012) after a careful evaluation of its performance based on determining sensitivity and uncertainty of a number of parameters in the model which directly or indirectly influence CH_4 production and emissions.

Uncertainty in CH_4 outputs will not only be a result of uncertain climate inputs or model parameters but will also depend on which fractional wetland map is used. To investigate the uncertainty of CH_4 emissions introduced by differing fractional wetland maps, three different fractional wetland maps will be applied in simulations for the same spatial domain.

The main goal of this thesis is to comprehensively evaluate the performance of LPJ-GUESS WHyMe on regional simulations.

2 Aim

There are 6 specific aims in this thesis, namely:

- To analyze the parameter sensitivity in the CH_4 module of LPJ-GUESS WHyMe and its influence on the output variables of CH_4 flux and CH_4 flux pathways, and further to identify the best overall parameter set for use in the Arctic tundra domain.
- To estimate CH_4 emissions by LPJ-GUESS WHyMe in Arctic tundra using different wetland maps, and to evaluate quantitative and qualitative differences in CH_4 flux based on these maps.
- To identify whether uncertain parameters or the influence of fractional wetland maps introduces more uncertainties when estimating methane emissions from Arctic tundra.

- To determine which pathways are dominant in methane transport from wetland to the atmosphere in Arctic tundra.
- To determine which environmental drivers are most important to the total CH_4 flux emitted from Arctic tundra and how these drivers varies over different seasons.
- To analyze the potential robust features in the model, and to identify their influence on modeling CH_4 flux in Arctic tundra.

3 Methods

In order to achieve the aims above, a working flowchart was planned and showed in Figure 1.

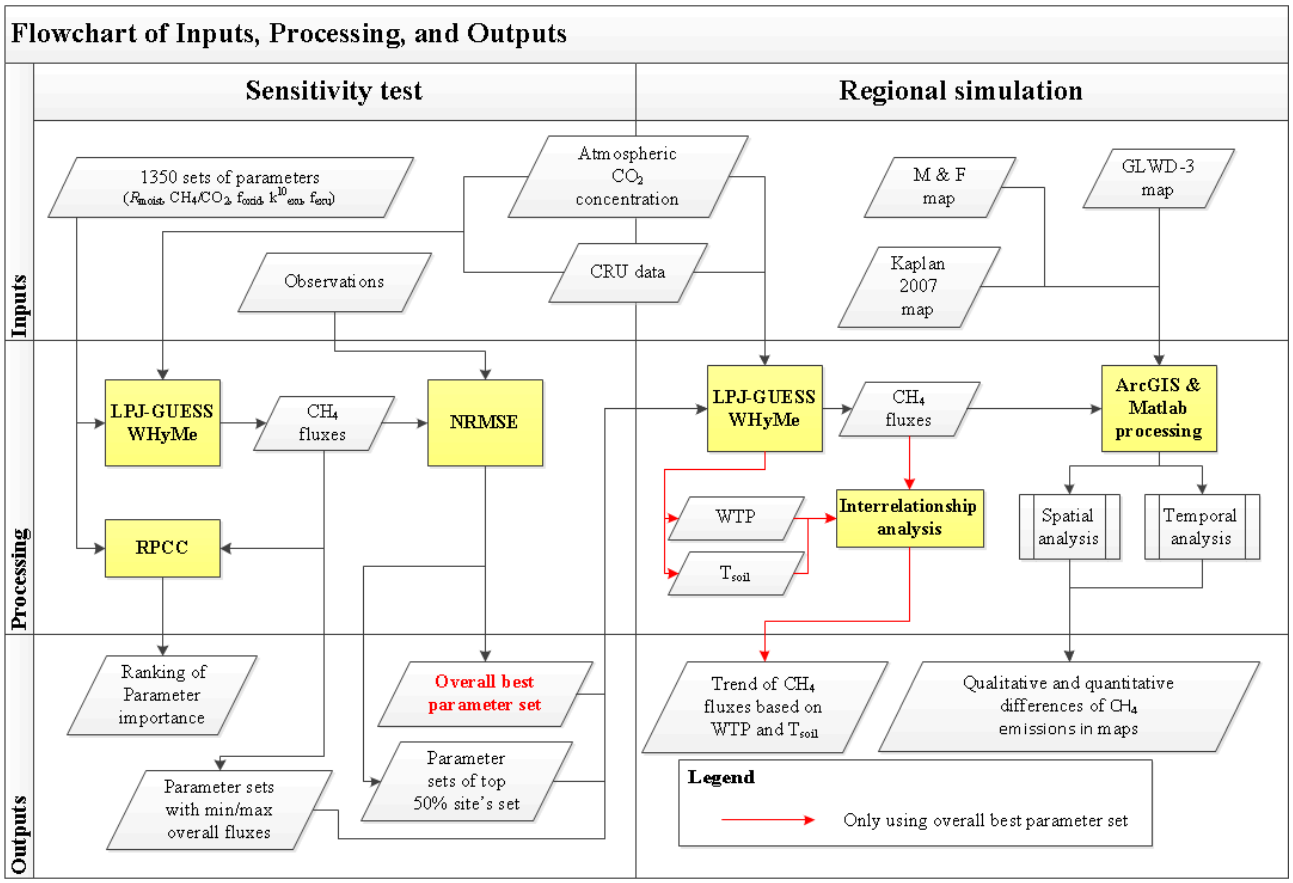

Figure 1. Flowchart of inputs, processing, and outputs in this modelling study.

3.1 Model description

LPJ-GUESS WHyMe (McGuire et al. 2012) is a development of the Lund-Potsdam-Jena General Ecosystem Simulator (LPJ-GUESS) incorporating both wetland hydrology and methane emissions process descriptions from LPJ-WHyMe (Wania et al. 2009).

As the basic framework of LPJ-GUESS WHyMe, LPJ-GUESS is a dynamic global vegetation model (DGVM) that simulates the structure and dynamics of terrestrial ecosystems at different

temporal and spatial scales. Physiological and biogeochemical processes of ecosystem are explicitly described in the papers Smith et al. (2001) and Sitch et al. (2003). The inputs to the model consist of climate data, atmospheric CO_2 concentrations and soil physical properties. At the same time, a set of plant functional types (PFTs) is necessary to define and characterize the bioclimatic niche, growth form, leaf phenology, photosynthetic pathway, and life history of modelled plant individuals. The simulated processes were explicitly described by Smith et al. (2001); the physiological processes (i.e. leaf photosynthesis and respiration), biophysical processes (i.e. energy and water exchange), and biogeochemical processes (i.e. carbon cycles) of ecosystems were described in the same way as LPJ-DGVM (Sitch et al. 2003). Standard outputs from the model include, carbon fluxes (NEE, NPP, GPP, autotrophic and heterotrophic respiration, fire disturbances, carbon stores (vegetation, soil, total carbon, root exudates, litter), biophysical properties (LAI, evapotranspiration, runoff, soil temperature and moisture). In our study, LPJ-GUESS was used in 'Cohort' (individual) mode. This mode has been shown to resolve more heterogeneity when simulating ecosystems at the landscape or continental scale due to its forest dynamic (gap) concept and the physical structure, competition, composition and distribution of vegetation through time are simulated in more realistic ways (Smith et al. 2001). In addition, some studies have shown that LPJ-GUESS had better performance comparing with LPJ at predicting potential natural vegetation (Smith et al. 2001; Hely et al. 2006).

The latest version of LPJ-WHyMe, 1.3.1, was described by Wania et al. (2010). The model is a development of LPJ, which is a process-based model that simulates vegetation physiology, carbon allocation, decomposition and hydrological fluxes of ecosystems (Sitch et al. 2003; Gerten et al. 2004). For the additional wetland hydrology model, permafrost and peatlands were firstly taken into account and introduced in LPJ (Wania et al. 2009a). Two new PFTs (flood-tolerant C_3 graminoids and *Sphagnum* mosses) and an inundation stress parameterization for all PFTs were also added (Wania et al. 2009b). The methane module of LPJ-WHyMe is generally separated into two parts: methane production and pathways of methane emission.

To produce methane, soil carbon inputs originate from daily net primary production (NPP), which partly turns over to a litter pool and an exudates pool (Figure 2). These litter and exudates then partly turnover to a potential carbon pool for methanogens. The process of [NPP – litter pool -fast/slow soil carbon pool] has already been described in LPJ model, where f is fraction of carbon used to turnover and k is turnover rate (Sitch et al. 2003). The process of [NPP – exudates pool – potential carbon pool for methanogens] is an addition in LPJ-WHyMe, where

f_{exu} is a fixed fraction indicating how much NPP is diverted into the exudates pool each day and k_{exu} is the exudate decomposition rate. Soil moisture content (R_{moist}) is a very important parameter controlling the establishment of the potential carbon pool for methanogens by (1):

$$k = k^{10} R_{\mathrm{T}} R_{\mathrm{moist}} \quad (1)$$

where k represents all turnover rates in the model (k_{litter} k_{fast} k_{slow} k_{exu}) in the process of [NPP – potential carbon pool for methanogens], k^{10} is the respective decomposition rate at 10°C, and R_T is an exponential function of soil temperature with a value of 1 at 10°C (Wania et al. 2010; Wania et al. 2009b). R_{moist} lies between 0 and 1 and is intended to reduce decomposition rates under inundation (Wania et al. 2010). In contrast to the description of the decomposition classified as heterotrophic respiration in LPJ, LPJ-Guess WHyMe considers the decomposed carbon in peatland first as a potential carbon pool for methanogens (Wania et al. 2010). The carbon in the potential carbon pool for methanogens is then allocated to each 0.1 m active soil layer, weighted by a prescribed root distribution (Wania et al. 2010). After the carbon has been allocated to each soil layer and decomposed, a fraction of the decomposed carbon is turned into methane ($Q_{methane}$) in each soil layer depending on the layer's anoxic fraction (f_{anoxic}, a function of the layer's soil water content), daily decomposition of the potential carbon pool for methanogens ($dPCP_{methane}$), and a parameter, methane/carbon dioxide (CH_4/CO_2) as (2).

$$\mathrm{Q}_{methane} = f_{anoxic} \times dPCP_{methane} \times [\mathrm{CH_4/CO_2}] \quad (2)$$

Each day, three pathways of methane transport (diffusion, plant-mediated transport and ebullition) are available to CH_4 in the soil. During methane transport in soil, a fraction of oxygen (f_{oxid}), which reaches each soil layer via diffusion and plant-mediated transport, oxidizes the methane in soil at each time step in a proportion of 1:2 moles as (3):

$$\mathrm{CH_4 + 2O_2 \rightarrow CO_2 + 2H_2O} \quad (3)$$

Wania et al. (2010) noticed that all methane would be oxidized if enough oxygen was available, otherwise, all oxygen would be used to oxidize methane.

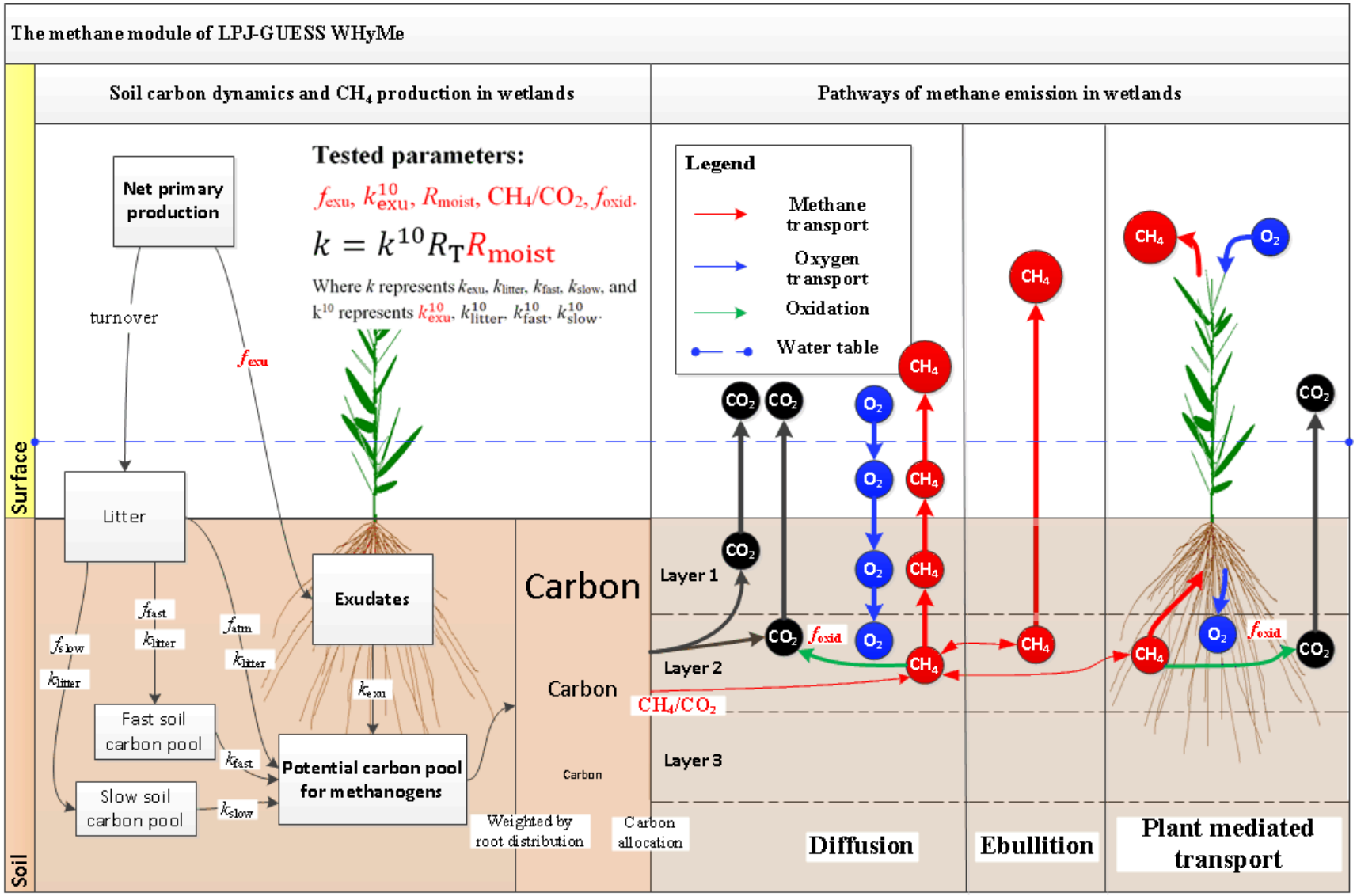

Figure 2. The methane module of LPJ-GUESS WHyMe.

A distinction between LPJ-WHyMe and other methane modelling approaches (Cao et al. 1996; Walter et al. 2001; Wania et al. 2010) is that LPJ-WHyMe takes account of changes in peatland vegetation since the methane model was simply added to LPJ-WHy as a separate sub-routine.

The version of LPJ-GUESS WHyMe used in this thesis uses the same description of wetland hydrology and the same methane subroutine as LPJ-WHyMe. For the hydrology scheme, the peatland soil is set to 2 m and is subdivided into an upper 0.3 m acrotelm (within which the water table is allowed to fluctuate) above a 1.7 m permanently saturated catotelm layer (McGuire et al. 2012). The water table is also allowed to extend above the soil surface to a maximum depth of 0.1 m, and its depth is updated daily in response to precipitation, snowmelt, evapotranspiration and surface runoff (McGuire et al. 2012). For the methane module, the ebullition description was modified to only operate when the soil temperature is above 0°C to avoid any unreasonable ebullition events in winter in the Arctic tundra domain. The methane module in LPJ-GUESS WHyMe used for simulating daily methane exchange can be generally summarized into 11 steps based on the order of processing: (1) C budget before today's methane calculations, (2) diffusivities and layer depths, and an update of gas constant settings, (3) calculate CH_4 and CO_2 production, (4) diffusion of O_2, (5) plant transport of O_2, (6) diffusion of CH_4, (7) CH_4 oxidation, (8) CH_4 diffusion from top layer after diffusion and oxidation, (9) plant transport of CH_4, (10) ebullition of CH_4, and (11) carbon conservation checks (Figure 2). The differences between two models are based on the differences between LPJ-GUESS and LPJ, i.e. the former simulates vegetation in the individual mode so that the processes of vegetation competition can be better presented.

In this study, input data for driving LPJ-GUESS WHyMe are climate data, atmospheric CO_2 concentration and wetland fraction maps. The climate data used in this thesis included monthly air temperature, cloud cover, precipitation and number of wet days in 1901-2009 on a $0.5^o \times 0.5^o$ spatial scale from the Climatic Research Unit time-series datasets CRU TS 3.10 (Harris et al. 2013; Mitchell & Jones 2005). Monthly atmospheric CO_2 concentration data for the period 1901-2001 were obtained from McGuire et al. (2001) and for the period 2002-2009 were based on observation from Mauna Loa Observatory (Hawaii) (Thoning et al. 2013). For each run, LPJ-GUESS WHyMe was run for a "spinup" phase of 500 years, which provides sufficient time to guarantee equilibrium of ecosystem carbon pools. In this phase, the first 30 years of CRU data (1901-1930) were continuously repeated and atmospheric CO_2 concentration was set at the same value as the first year (1901). Five replicate patches, of area 1000 m^2 each, were

simulated, which were used to account for heterogeneity resulting from stochastic plant establishment, mortality and disturbances.

3.2 Site test/Observations

In order to compare with the results from Wania et al. (2010) and fit parameters for the Arctic tundra area, five northernmost sites of the seven sites used in the Wania et al. (2010) study were used (Table 1 & Figure 3). The two unused sites are below 45ºN.

Since the observations were taken on point sites, the microclimates on sites are usually not completely in agreement with regional climate on 0.5º × 0.5º spatial scale, which is the basic grid cell in CRU data. Therefore, in order to make simulations and observations in comparable, the CRU data had to be adjusted to match observed climate data from each of the five sites before it forced the model simulations. Compared with other climate input, air temperature and precipitation are the two most effective inputs on CH_4 emissions simulations (Gedney et al. 2004), so adjustments for these two climate variables were completed for all five observation sites (Table 1).

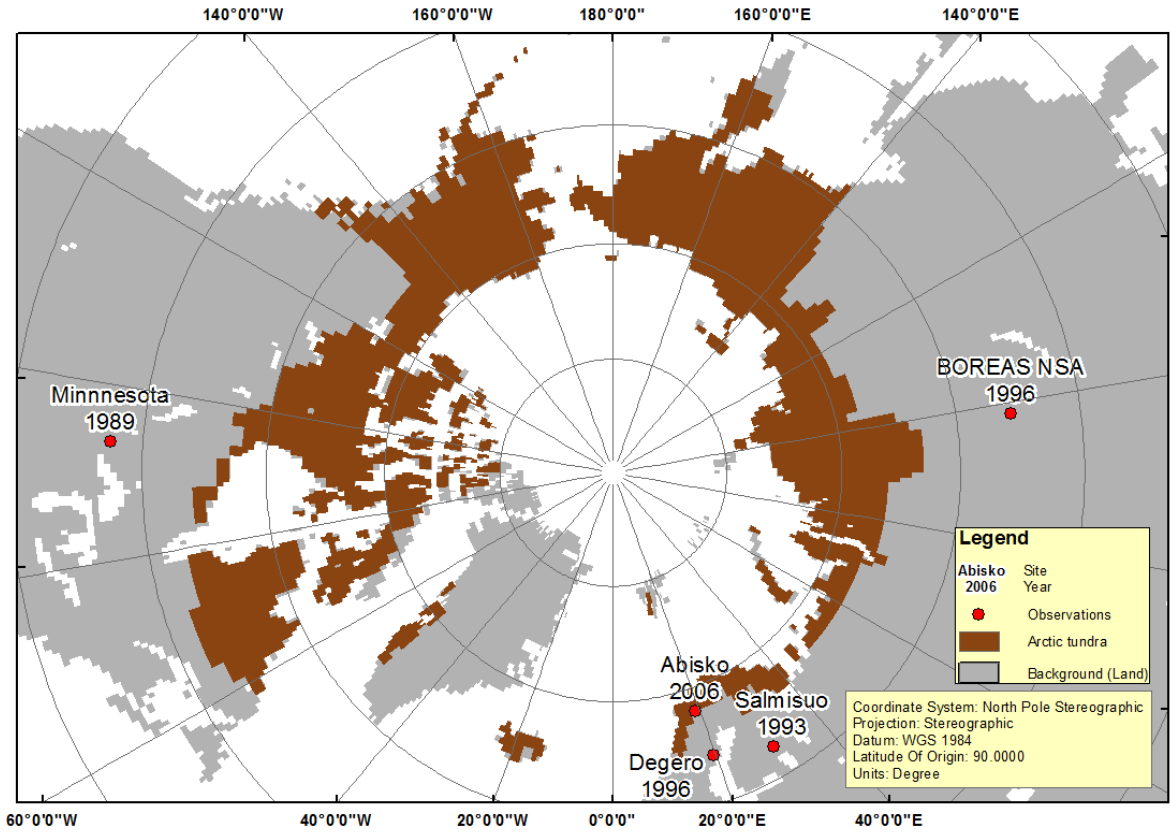

Figure 3. Observations and Arctic tundra.

Table 1. Observational sites used for sensitivity testing.

No.	Site name	Coordinate	Year[a]	Type	Vegetation	T/P [b]	Method	Ref.
1	Minnesota USA	47.5ºN 93.5ºW	1989	Poor fen	Sedge (*Carex oligosperma* Michaux); Arrow-grass (*Scheuchzeria palustris*); Cranberry (*Vaccinium oxycoccus*); *Sphagnum angustifolium* (C. Jens. Ex Russ) C. Jens.; S. *capillifolium* (Ehrh.) Hedw.; S. *fuscum* (Schimp.) Klinggr.	-0.57/1.09	Chamber	Dise (1993)
2	BOREAS NSA Canada	55.5ºN 98.5ºW	1996	Fen	Peat mosses (*Sphagnum* spp.); Brown moss (*Drepandocladus exannulatus* (B.S.G) Warnst.); Bogbean (*Menyanthes trifoliate* L.); Sedges (*Carex* spp.); Larch (*Larix laricina* (Du Roi) K. Koch); Bog birch (*Betula glandulosa* Michx.).	0.0/1.06	Chamber	Bubier et al. (1988)
3	Salmisuo Finland	62.5ºN 30.5ºE	1993	Fen	Cottongrass (*Eriophorum vaginatum* L.); Bog-rosemary (*Andromeda polifolia* L.); Cranberry (*Vaccinium oxycoccus*); Sedge (*Carex pauciflora* Lightf.); *S. angustifolium* (Russow) C. Jens.; *S.balticum* (Russow) C. Jens.; *S. magellanicum* Brid.; *S. papillosum* Lindb.	-0.44/1.05	Chamber	Thoning et al. (2013)
4	Degerö Sweden	64.0ºN 19.5ºE	1996	Poor fen	Cottongrass (*Eriophorum vaginatum*); Cranberry (*Vaccinium oxycoccus*); Bog-rosemary (*Andromeda polifolia*); Arrow-grass (*Scheuchzeria palustris*); Sedge (*Carex limosa* L.); *Sphagnum balticum*; *S. majus* (Russ.) C. Jens.; *S. lindbergii* Schimp.	1.24/0.85	Chamber	Granberg et al. (2001)
5	Abisko Sweden	68.0ºN 19.0ºE	2006	Mire	Cottongrass (*Eriophorum vaginatum*); Brown moss (*Drepanocladus* sp.).	3.22/0.47	Eddy covariance	Jackowicz-Korczynski et al. (2010)

[a] Year of observation data used.
[b] Temperature (+) and precipitation (×) adjustment to climate forcing from CRU.

3.3 Sensitivity test

Five parameters (R_{moist}, CH_4/CO_2, f_{oxid}, k_{exu}^{10}, and f_{exu}) (Table 2) were selected for CH_4 sensitivity testing based on the results of sensitivity tests with seven parameters in the Wania et al. (2010) study, which showed that CH_4/CO_2 was the most important parameter, followed by R_{moist} and f_{oxid}. Values of these parameters were set manually. The more important parameters had more values to test (Table 3). For all of the possible 1350 different combinations in parameter space, the Ranked Partial Correlation Coefficient (RPCC) method, the statistical approach of Vogelmann et al. (2001) and Wramneby et al. (2008), was used to analyze the parameter influence on monthly total CH_4 fluxes and the monthly CH_4 fluxes following the three pathways. This approach was accomplished by two main sub-approaches: (i) the Partial Correlation Coefficient (PCC), which defined as the correlation coefficient between $x_j - \hat{x}_j$ and $y - \hat{y}$, was calculated to identify how uncertainty of each parameter contributed to uncertainty of the output variable (Zaehle et al. 2005). x_j and y were a specific parameter and output variable respectively, and $\hat{x}_j$ and $\hat{y}$ were calculated from following formulas:

$$\hat{x}_j = a_0 + \sum_{\substack{p=1 \\ p \neq j}}^{n} a_p x_p \quad (4)$$

and

$$\hat{y} = b_0 + \sum_{\substack{p=1 \\ p \neq j}}^{n} b_p x_p \quad (5)$$

These two formulas can provide a single linear relationship between x_j and y when the output variable y is influenced by other factors; (ii) Rank-transformation was used for repeatedly analyzing the PCC based on assuming that a single parameter provided monotonic effect on output variables, due to parameters and output variables were possibly in a non-linear relationship. In this study, the RPCC approach was used to identify the influence of the five selected parameters on CH_4 fluxes in different locations, in different time periods, and from different pathways.

Table 2. Sensitivity test parameters (Wania et al. 2010).

$\boldsymbol{R_{moist}}$	Moisture response, used to weight decomposition rates for exudates, litter, fast and slow carbon pools – see equation 1
$\boldsymbol{CH_4/CO_2}$	CH_4/CO_2 production ratio under anaerobic conditions – see equation 2
$\boldsymbol{f_{oxid}}$	Fraction of available oxygen used for methane oxidation – see equation 3
$\boldsymbol{k_{exu}^{10}}$	Exudate decomposition rate at 10 °C (a^{-1})
$\boldsymbol{f_{exu}}$	Fraction of NPP put into exudates pool

Table 3. Values for the parameter sensitivity test and parameter optimization. There are 5×6×5×3×3=1350 possible parameter combinations in total.

Parameters	Value					
R_{moist}	0.2	0.3	0.4	0.5	0.6	
CH_4/CO_2	0.05	0.1	0.15	0.2	0.25	0.3
f_{oxid}	0.5	0.6	0.7	0.8	0.9	
k_{exu}^{10} [a]	13	26	39			
f_{exu} [b]	0.0875	0.175	0.2625			

[a] k_{exu}^{10} is set at 26 (2 weeks) as a default value.
[b] f_{exu} is set at 0.175 as a default value (Wania et al. 2009b).

3.4 Parameter optimization

For each observation site (Table 1), the best site parameter set was determined by using the root mean square error (RMSE), which is the same as the method used in Wania et al. (2010), between monthly modelled CH_4 fluxes and monthly observations. The RMSE was calculated from:

$$RMSE = \sqrt{\frac{\sum_{i=1}^{n}(M_i - O_i)^2}{n}} \quad (6)$$

where *M* is modelled and *O* is observed CH_4 flux; n is the number of observed months.

In order to compare error from all sites, the RMSE was normalized (NRMSE) by the standard deviation of observations σ_O.

$$NRMSE = RMSE/\sigma_O \quad (7)$$

Normally, the best overall parameter set is determined by selecting the lowest average NRMSE from all observation sites (Wania et al. 2010). This traditional method could possibly lead to a best overall parameter set being one with a very low error at a particular observation site but with a large error at another observation site. In order to avoid this extreme situation, the best overall parameter set with the lowest average NRMSE was calculated using the best 50% (1350/2) of parameter sets in each site. Finally, the best overall parameter set determined in this way was applied in the regional simulation.

3.5 The Arctic tundra boundary and wetland fraction maps

3.5.1 The Arctic tundra boundary

The study area (Arctic tundra) boundary was defined by the Regional Carbon Cycle Assessment and Processes (RECCAP) Activity (McGuire et al. 2012). McGuire et al. (2012)

noticed that the spatial domain of Arctic tundra extends into the boreal forest in some areas, for example in western North America. All wetland fraction maps (Kaplan 2007, Matthews and Fung, GLWD-3) used this boundary and were processed to the same spatial resolution as the climate data, which was at a 0.5-degree spatial resolution.

3.5.2 Wetland map by Kaplan (2007)

The Kaplan 2007 Global Wetlands Dataset is a global wetlands map, which was assembled by using the best available sources of large-scale wetland cover information for each continent or region at spatial resolutions from 30 m to 5-minute (Bergamaschi et al. 2007). In detail, for the dataset, Bergamaschi et al. (2007) used five major data sources to calculate the fractional cover of wetland area on a spatial resolution of 0.5-degree: (1) the vector Canadian Peatlands Database for Canada (Tarnocai et al. 2000), (2) the 30 m U.S. National Land Cover Dataset for the conterminous United States (Vogelmann et al. 2001), (3) the 1 km native resolution GLC2000 global land cover dataset for South America, Africa, Eastern Europe and northern Asia (JRC, 2003), (4) the 250 m Corine Land Cover 1990 dataset for Europe (ETCTE, 2000), and (5) the 5' WELAREM1 database of global wetlands for all other regions (Lehner and Döll, 2001).

3.5.3 Wetland map by Matthews and Fung

The map of Matthews and Fung (1987) is a global data base of wetlands at 1-degree resolution integrated from three independent digital sources: (1) vegetation classified using the United Nations Educational Scientific and Cultural Organization (UNESCO) system (Matthews 1983), (2) soil properties from the Food and Agriculture Organization (FAO) soil maps (Zobler, 1986), and (3) fractional inundation at 1-degree resolution from a global map survey of Operational Navigation Charts (ONC). Since the spatial resolution of the map was lower than that of the climate data, it was increased to agree with the spatial resolution of the climate data at 0.5-degree.

3.5.4 Global Lakes and Wetlands Database-Level 3

Drawing upon a variety of existing maps, data and information, Lehner and Döll (2004) created the Global Lakes and Wetlands Database (GLWD) by applying a Geographic Information System (GIS) approach to combine seven different data set for lakes and wetlands: (1) MSSL Global Lakes Database (MGLD) (Birkett & Mason 1995), (2) Data set of Large Reservoirs (LRs) (Vorosmarty et al. 1997), (3) The world register of Dams (WRD) (ICOLD, 1988, 1998), (4) The Digital Chart of the World (DCW) (ESRI, 1993), (5) ArcWorld 1:3M data set (ESRI,

1992), (6) Wetlands map of the World Conservation Monitoring Center (WCMC) wetlands map (Dugan, 1993; WCMC, 1993), and (7) USGS Global Land Cover Characteristics (GLCC) database in 'Global Ecosystem' classification (Loveland, 1991; Loveland et al, 2000). GLWD provides a representation of water bodies in three levels: (1) large lakes and reservoirs, (2) smaller water bodies, and (3) wetlands. In this study, level 3 (GLWD-3) was used; it provides 12 classes of water bodies in a global raster map at 30-second resolution.

In order to be comparable to the other two maps, GLWD-3 map was clipped to the Arctic tundra boundary and was aggregated to 0.5-degree resolution. To calculate the wetland fraction in each pixel, according to the assessment of GLWD-3 for wetland, class 1, 2 and 3, which are not wetland areas, were not used; class 10 (50-100% wetland) was set to 100% for adjusting the Arctic tundra wetland area in Alaska (Lehner & Döll 2004); class 11 (25-50% wetland) was set to 25% for adjusting the Arctic tundra wetland area in Canada (Lehner & Döll 2004); class 12 (wetland complex) was set to 12.5%, which is the average of the range; and other classes were reclassified as 100% (Table 4).

Table 4. Classification in GLWD-3 and wetland fraction setting for Arctic tundra (Lehner & Döll 2004).

Id	GLWD-3 Class	Fraction in processing
1	Lake	-
2	Reservoir	-
3	River	-
4	Freshwater March, Flood plain	100%
5	Swamp Forest, Flooded Forest	100%
6	Coastal Wetland	100%
7	Pan, Brackish/Saline Wetland	100%
8	Bog, Fen, Mire	100%
9	Intermittent Wetland/Lake	100%
10	50-100% Wetland	100%
11	25-50% Wetland	25%
12	Wetland Complex (0-25%)	12.5%

3.6 Regional simulation

After optimizing the parameter set and setting the boundary of Arctic tundra, and in order to decrease the computational time, a single regional simulation driven by climate data for the period of 1901-2009 was run using LPJ-GUESS WHyMe with the assumption of a 100% wetland fraction in all pixels in the tundra domain. The regional CH_4 emissions were then

estimated in a post-processing step by multiplying the wetland fraction from the three fractional maps by the CH_4 fluxes from this simulation.

In order to detect the changes of CH_4 emissions between the climate standard period (1961-1990) and the following period (1991-2009), each pixel's differences (Δ) in two periods were normalized following:

$$\Delta = (E_1 - E_0)/E_0 \quad (5)$$

where E_1 was the average annual CH_4 emissions in 1991-2009; E_0 was the average annual CH_4 emissions in the climate standard period (1961-1990); $\Delta=0$ means no change, $\Delta>0$ means CH_4 emissions increase, and $\Delta<0$ means CH_4 emissions decrease.

A comparison among three different fractional wetland maps was focused on dynamic uniformity and quantitative differences. Water table position and near-surface soil temperature have been shown to be strongly related to CH_4 production (Hargreaves & Fowler 1998; Moore & Roulet 1993); therefore, the most effective factors, water table position and soil temperature at 25 cm, were used in a visually qualitative analysis of their influences on regional CH_4 fluxes.

In addition, in order to detect whether the influence of parameters or the influence of fractional wetland maps provides more uncertainty when estimating methane emissions from Arctic tundra, a relative uncertainty and an absolute uncertainty caused by parameter uncertainty was determined. A relative uncertainty was set through estimating CH_4 emission using the common parameter sets in the best 50% parameter sets in each site, and an absolute uncertainty was defined through estimating CH_4 emission using two parameter sets, which were determined by minimum and maximum total CH_4 fluxes from five observation sites. The Arctic tundra wetland CH_4 emissions with these parameter sets was simulated by using the three fractional wetland maps, and evaluated whether parameters or wetland maps introduce more uncertainty to the regional CH_4 simulations.

Table 5. RPCC of parameters and annual methane emission for each test site, in two different periods.

	Parameters	1961-1990					1991-2009				
		R_{moist}	CH_4/CO_2	f_{oxid}	k_{exu}^{10}	f_{exu}	R_{moist}	CH_4/CO_2	f_{oxid}	k_{exu}^{10}	f_{exu}
Minnesota	Total	-0.313	0.999**	-0.851	0.090	-0.923*	-0.230	0.997**	-0.875*	0.227	-0.647
	Diffusion	-0.314	0.999**	-0.869	0.143	-0.919*	-0.351	0.998**	-0.906*	0.275	-0.238
	Ebullition	0.192	0.987**	-0.255	-0.049	-0.603*	0.240	0.956**	-0.156	-0.008	-0.387*
	Plant mediated	-0.294	0.998**	-0.814	0.057	-0.916*	-0.298	0.995**	-0.676	0.099	-0.681*
BOREAS	Total	-0.393	0.998**	-0.888*	-0.028	-0.850	-0.266	0.998**	-0.875*	-0.018	-0.838
	Diffusion	-0.421	0.998**	-0.917*	-0.024	-0.835	-0.316	0.998**	-0.906*	-0.007	-0.827
	Ebullition	0.678*	0.692**	-0.029	0.000	-0.028	0.714**	0.713*	-0.048	0.010	-0.113
	Plant mediated	-0.417	0.998**	-0.722	-0.045	-0.894*	-0.266	0.998**	-0.696	-0.040	-0.882*
Sallmisuo	Total	0.466	0.964**	-0.280	0.004	-0.929*	0.425	0.957**	-0.255	0.004	-0.906*
	Diffusion	0.437	0.971**	-0.327	0.008	-0.929*	0.418	0.970**	-0.324	0.011	-0.918*
	Ebullition	0.245	0.979**	-0.196	-0.018	-0.749*	0.138	0.891**	-0.087	-0.010	-0.279*
	Plant mediated	0.456	0.924**	-0.163	-0.003	-0.913*	0.373	0.895**	-0.141	-0.005	-0.872*
Degerö	Total	0.039	0.999**	-0.939*	-0.070	-0.202	-0.014	0.999**	-0.919*	-0.055	-0.353
	Diffusion	-0.121	0.999**	-0.944*	-0.049	0.033	-0.141	0.998**	-0.926*	-0.040	-0.265
	Ebullition	0.306*	0.984**	-0.225	-0.019	0.060	0.411*	0.953**	-0.175	-0.010	-0.013
	Plant mediated	0.158	0.998**	-0.792*	-0.093	-0.549	0.198	0.998**	-0.824*	-0.129	-0.763
Abisko	Total	0.060	0.999**	-0.931*	-0.076	-0.253	0.059	0.999**	-0.918*	-0.068	-0.164
	Diffusion	-0.010	0.999**	-0.935*	-0.070	-0.165	0.005	0.998**	-0.924*	-0.063	-0.132
	Ebullition	1.000**	-0.024*	-0.005	0.000	0.000	0.984**	0.217*	-0.049	-0.002	0.179
	Plant mediated	0.232	0.999**	-0.829*	-0.082	-0.486	0.430	0.999**	-0.910*	-0.138	-0.669

**: Rank 1

*: Rank 2

4 Results

4.1 Sensitivity test

A RPCC table presents the PCC of five parameters with pathway and total CH_4 fluxes at five observed sites in two periods: the climate standard period 1961-1990 & the following period 1991-2009 (Table 5).

For the total CH_4 fluxes from three pathways, as well as the diffusive CH_4 fluxes, the parameter CH_4/CO_2 provides the most important positive influence at all sites in both periods. The second most important parameter is different among sites: f_{exu} for Minnesota and Sallmisuo and f_{oxid} for BOREAS, Degerö, and Abisko, though the parameter f_{oxid} becomes the second most important at Minnesota during 1991-2009 instead of f_{exu}. The parameter ranking of influence on the plant mediated transport CH_4 fluxes is very stable, with the parameter CH_4/CO_2 still playing the most important role in all five sites and in both periods. The second ranking parameter is different among sites but does not change with time. For the ebullition CH_4 fluxes, more complex variances of parameter ranking exist among sites and periods. R_{moist} plays a more important role, with extremely RPCC high values at Abisko site in both periods. Similarly, R_{moist} becomes the highest ranked parameter at BOREAS in 1991-2009.

4.2 Parameter fitting

The sites' best parameters and the overall best parameters are shown in Table 6, which shows the overall best parameters in Wania et al. (2010) for comparison. After the parameter optimization method was used to identify the lowest NRMSE parameter set in the top 50% sets at all sites, only 12 co-sets of parameters were found and are shown in Table 7. In these 12 parameter sets, values of R_{moist}, CH_4/CO_2, and f_{exu} do not change, and the variable parameters are only f_{oxid} and k_{exu}^{10}, which have value changes completely covering their testing ranges. Comparing with observations of CH_4 fluxes at these five sites, LPJ-GUESS WHyMe shows the best performance at Salmisuo; the NRMSE of the site best parameter set is 0.31 and of the overall best parameter set is 0.33; the worst performance is at BOREAS, where NRMSE are high: 0.87 and 1.27 for the site best and overall best parameter sets (Figure 4). The modelled CH_4 fluxes at five sites using the overall best parameter set are found both above (BOREAS, Salmisuo and Abisko) and below (Minnesota and Degerö) the modelled fluxes given by the site best parameter set (Figure 4). Modelled CH_4 emission by the overall best parameter set for

the only site situated in Arctic tundra, Abisko, is underestimated (Figure 4). More detail for comparison of observation and simulation is shown in Figure 5. NRMSE shows how points are close to the 1:1 lines, and the coefficient of determination between observed and modelled (R^2) shows how points are close to the trend lines (Figure 5).

Table 6. The sites-specific best parameter set and the overall best parameter sets.

Parameters	Site best					Overall best	
	Minnesota	BOREAS	Salmisuo	Degeroe	Abisko	Wania/McGuire[d]	Final value[a]
R_{moist}	0.6	0.6	0.2	0.6	0.6	0.4/0.4	0.2
CH_4/CO_2	0.1	0.2	0.2	0.15	0.3	0.1/0.25	0.2
f_{oxid}	0.5	0.6	0.5	0.5	0.6	0.5/0.9	0.7
k_{exu}^{10} [b]	39	39	39	39	13	13/26	39
f_{exu}[c]	0.2625	0.0875	0.175	0.0875	0.0875	0.15/0.175	0.175

[a] Minimum NRMSE in the best 50% RMSE in each site.
[b] k_{exu}^{10} was set at 26 (2 weeks) as a default value.
[c] f_{exu} was set at 0.175 as a default value.
[d] Values used by Wania et al. (2010) and McGuire et al. (2012).

Table 7. The best parameter sets in the top 50% ranking.

No.	R_{moist}	CH_4/CO_2	f_{oxid}	k_{exu}^{10} [a]	f_{exu}[b]	NRMSE
1	0.2	0.2	0.6	13	0.175	0.865
2	0.2	0.2	0.6	26	0.175	0.860
3	0.2	0.2	0.6	39	0.175	0.859
4	0.2	0.2	0.7	13	0.175	0.859
5	0.2	0.2	0.7	26	0.175	0.857
6*	**0.2***	**0.2***	**0.7***	**39***	**0.175***	**0.856***
7	0.2	0.2	0.8	13	0.175	0.867
8	0.2	0.2	0.8	26	0.175	0.867
9	0.2	0.2	0.8	39	0.175	0.865
10	0.2	0.2	0.9	13	0.175	0.881
11	0.2	0.2	0.9	26	0.175	0.873
12	0.2	0.2	0.9	39	0.175	0.869

* Best overall parameter set used in this study.
[a] k_{exu}^{10} is set at 26 (2 weeks) as a default value.
[b] f_{exu} is set at 0.175 as a default value (Wania et al. 2009b).

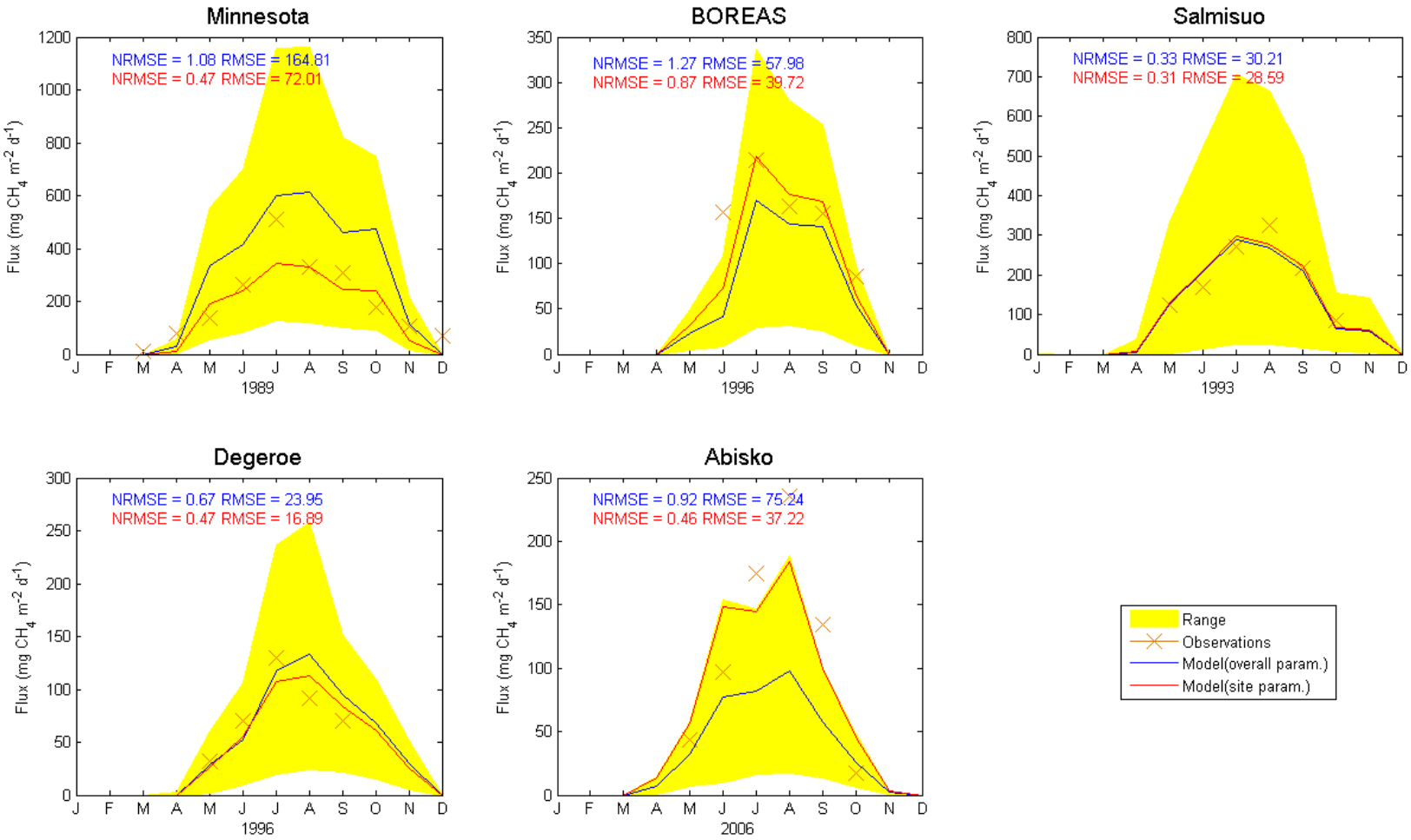

Figure 4. Modelled daily methane fluxes with all tested parameter sets compared to observations for five sites.

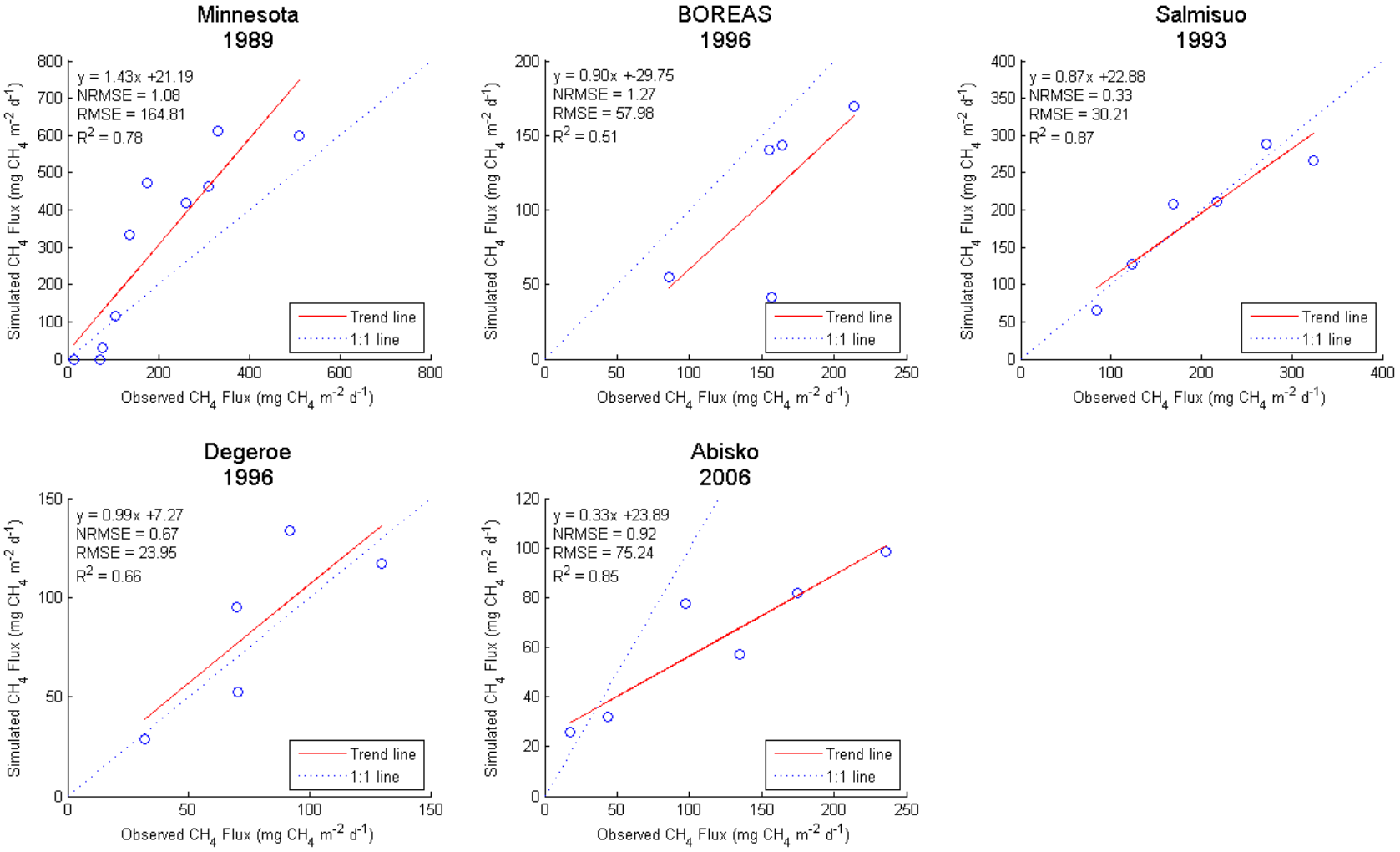

Figure 5. Modelled daily methane fluxes with the best overall parameter sets compared to observations for five sites.

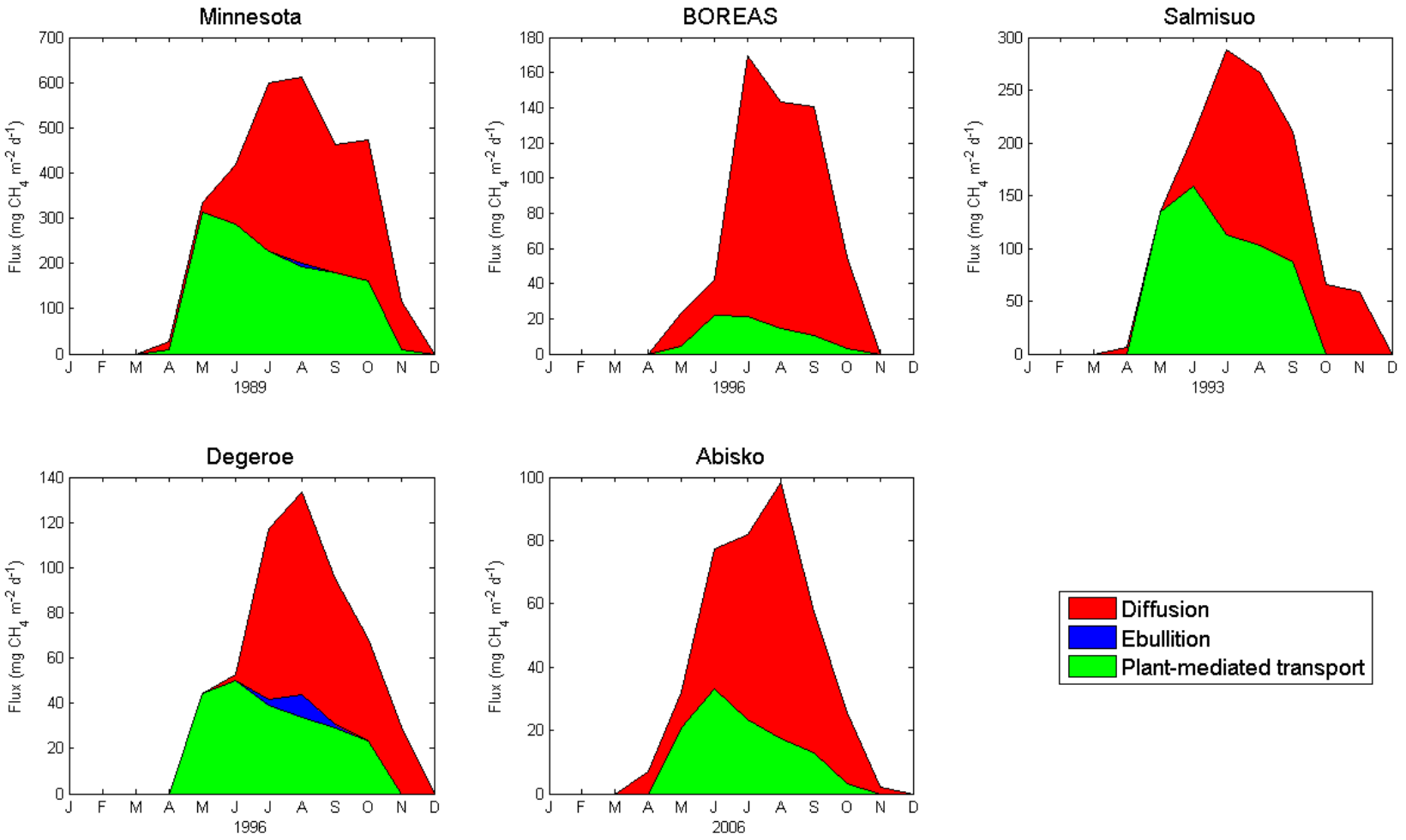

Figure 6. Modelled daily methane fluxes displayed by three transport pathways for five observed sites using the best overall parameter set.

Using the overall best parameter set, three different transport pathways of CH_4 fluxes for five sites are plotted in Figure 6. Diffusion contributes the largest amount to CH_4 fluxes; plant-mediated emissions follow; and ebullition contributes the least, with no ebullition at BOREAS, Salmisuo, and Abisko (Figure 6 & Table 8). Plant-mediated emissions display obvious seasonal variances and the peaks always exist in May or June; however, diffusion seems to have a seasonal shift with the peaks always existing in July or August (Figure 6). Similarly, the peak of ebullition displays in August. Minnesota and Salmisuo have very significant plant-mediated emissions, which are both over 45% of total emissions (Table 8). Furthermore, the annual NPP of WetGRS in these two sites is much larger than that of moss (Table 9). Compared with the estimations in the Wania et al. (2010) study, the most significant difference is the balance between diffusion and plant-mediated transport, with diffusion being larger than plant-mediated transport in the simulations for this thesis (Table 8).

Table 8. Modelled total and transport pathway methane fluxes ($gCH_4\ m^{-2}\ yr^{-1}$) from five sites using the best overall parameter set.

Site	Year	Diffusion		Ebullition		Plant		Total
Minnesota	1989	50.84	(54.4%)	0.27	(0.3%)	42.29	(45.3%)	93.40
-	-	6.53	(22.9%)	0.11	(0.4%)	21.88	(76.7%)	28.54
*	*	66.58	(54.9%)	1.96	(1.6%)	52.70	(43.5%)	121.24
BOREAS	1996	15.30	(87.0%)	0.00	(0.0%)	2.30	(13.0%)	17.60
-	-	4.80	(29.2%)	0.14	(0.9%)	11.49	(69.9%)	16.43
*	*	20.02	(87.0%)	0.00	(0.0%)	3.00	(13.0%)	23.02
Salmisuo	1993	19.69	(52.0%)	0.00	(0.0%)	18.19	(48.0%)	37.88
-	-	11.17	(30.9%)	0.49	(1.4%)	24.51	(67.8%)	36.16
*	*	26.84	(52.3%)	1.35	(2.6%)	23.09	(45.0%)	51.28
Degerö	1996	9.43	(56.8%)	0.44	(2.6%)	6.73	(40.5%)	16.60
-	-	6.76	(25.7%)	0.22	(0.8%)	19.58	(74.3%)	26.35
*	*	12.88	(58.1%)	1.75	(7.9%)	7.54	(34.0%)	22.17
Abisko	2006	8.29	(71.0%)	0.00	(0.0%)	3.39	(29.0%)	11.68
-	-	1.38	(15.5%)	0.00	(0.0%)	7.52	(84.5%)	8.90
*	*	11.75	(71.0%)	0.00	(0.0%)	4.80	(29.0%)	16.55

Note: (a) the second lines (-) of each site are estimated in the Wania et al. (2010) study; (b) the third lines (*) of each site are simulated by parameter set optimized in the McGuire et al. (2012) study; (c) Percentage values in parentheses show the contribution of each pathway flux to the total flux.

Table 9. Modelled annual net primary production (NPP), gC m^{-2} yr^{-1}, of each LPJ-GUESS WHyMe PFT in the observed year, using the best overall parameter set.

Site	Year	WetGRS[a]	Moss[b]	Total
Minnesota	1989	353	49	402
BOREAS	1996	0	108	108
Salmisuo	1993	279	75	354
Degerö	1996	0	182	182
Abisko	2006	-1	118	117

[a] Cool, flood-tolerant (C3) grass
[b] Sphagnum spp.

4.3 Arctic tundra simulation

Three maps GLWD-3, Mathews & Fung, and Kaplan were processed at the same spatial resolution of 0.5 degree. All maps shows that most of tundra wetlands are concentrated between 65°N-70°N (Figure 7), especially in northern Alaska (Figure 8). GLWD-3 shows a large amount of wetlands between 60°N-65°N and around 55°N, where southern Alaska, southern east Siberia, and central Canada contribute the most (Figure 7 & Figure 8). Kaplan also shows large fractions of wetland in central Canada, but not in southern Alaska and southeast Siberia, which results in low wetland area between 55°N-65°N (Figure 7 & Figure 8). The map of Mathews & Fung shows low wetland area below 65°N (Figure 7), but seems to have larger wetland area in west Siberia (Figure 8). Summing across the domain, the area of wetland estimated from GLWD-3, at 14.5% of Arctic tundra, is almost twice the area of wetland from Matthews and Fung or Kaplan 2007, which are very close to each other (Table 10).

Table 10. The arctic tundra zonal wetland area for the three maps used in this study.

Map	Area (km^2) $\times 10^6$
GLWD-3	1.27(14.5%)
Matthews and Fung	0.69(7.9%)
Kaplan 2007	0.68(7.8%)
Tundra total	8.75

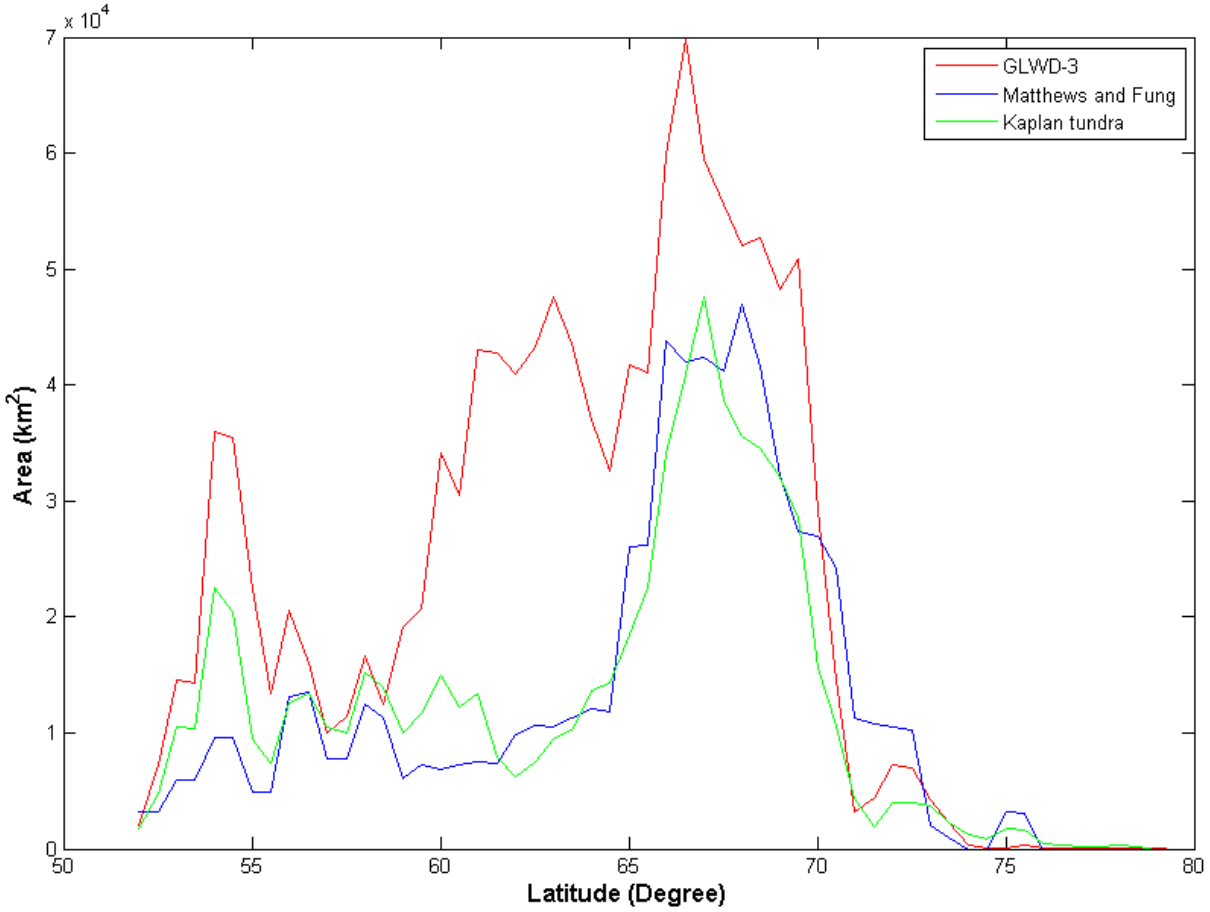

Figure 7. The arctic tundra zonal wetland area for the three maps used in this study.

Simulated average annual CH_4 fluxes from wetland for three maps in the climate standard period (1961-1990) show a very significant latitudinal gradient from the north to the south (Figure 9). The map of Matthews and Fung contains the least information of the three maps. Even if GLWD-3 shows larger area than Kaplan, Kaplan contains the most complete information, especially for the whole of Siberia and Scandinavia (Figure 9). High flux regions are mainly located in southern Alaska, eastern Canada, Iceland, northern Scandinavia, central Siberia and southeastern Siberia (Figure 9).

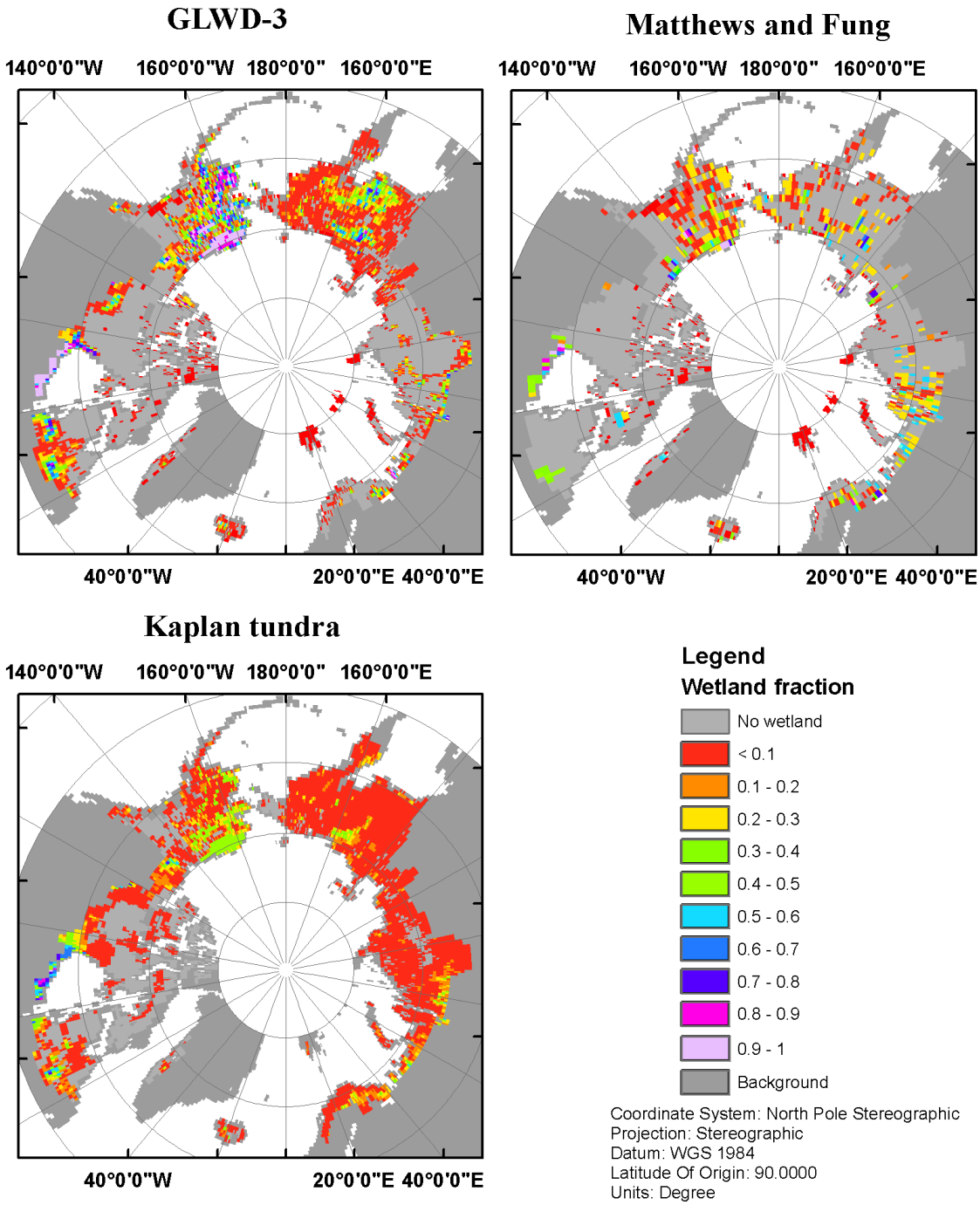

Figure 8. Fraction distributions of the three wetland maps used in this study.

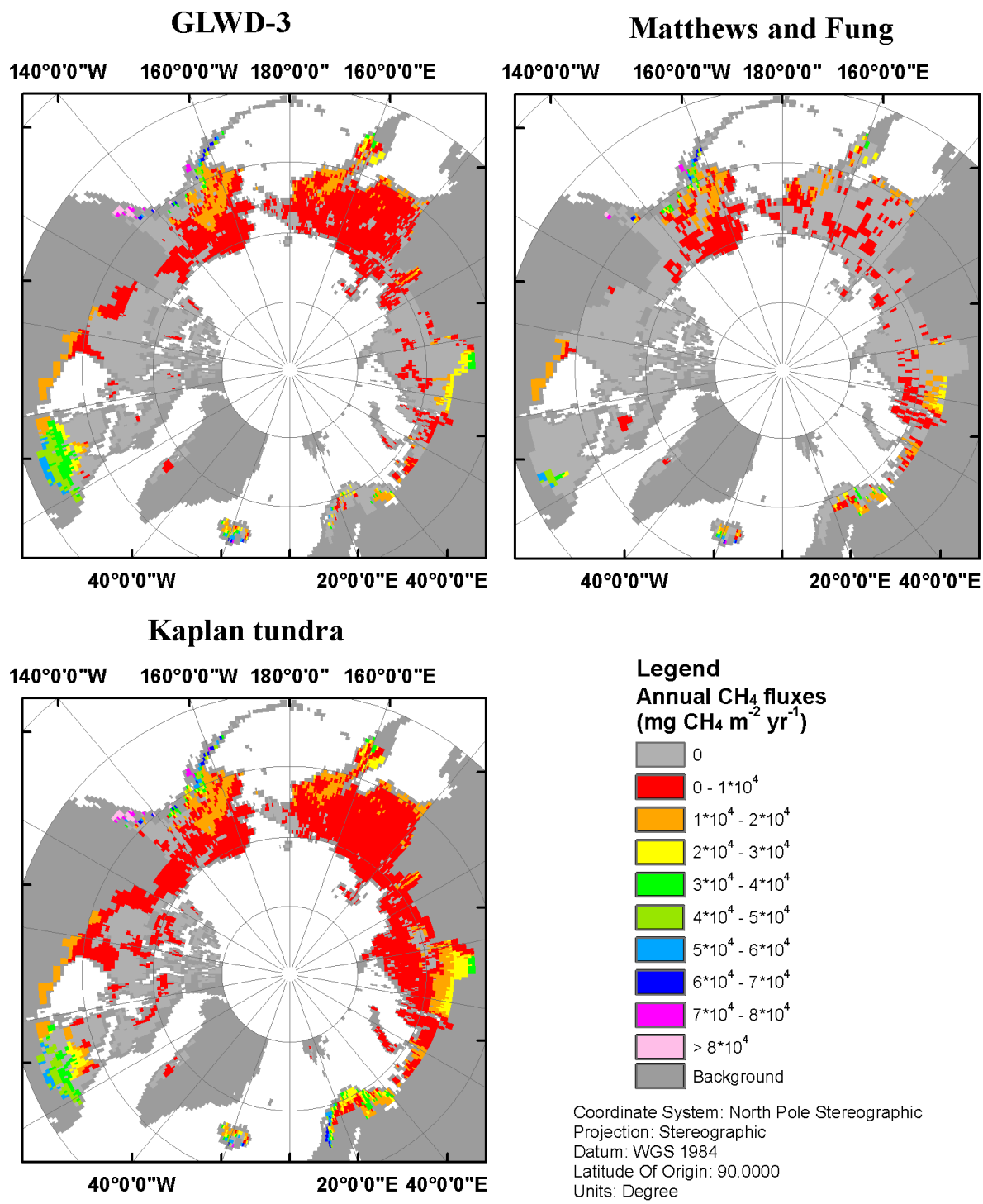

Figure 9. Simulated average annual methane fluxes from wetlands for three maps in 1961-1990 using the best parameter set.

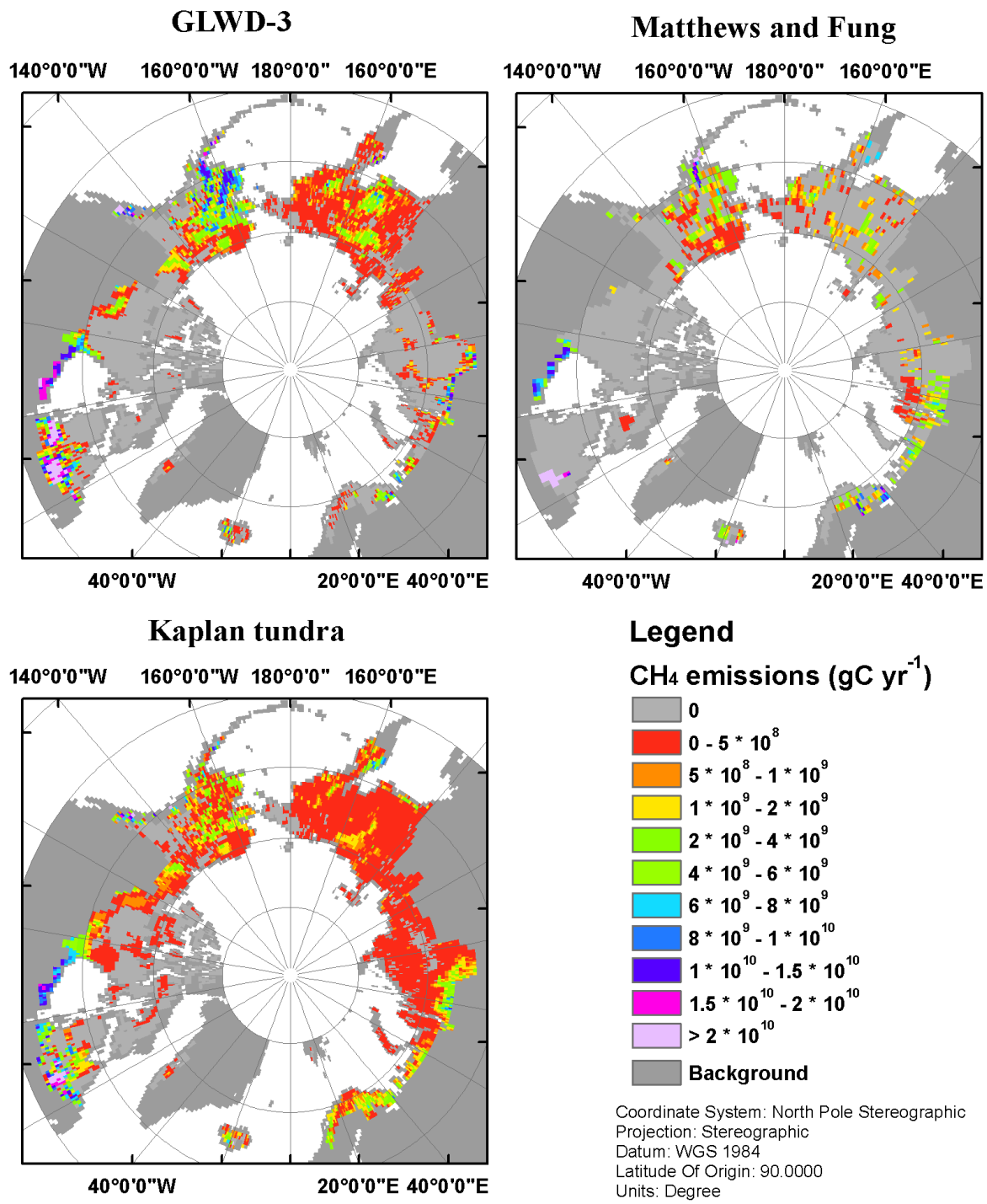

Figure 10. Simulated average annual CH_4 emissions for three maps in 1961-1990 using the best parameter set.

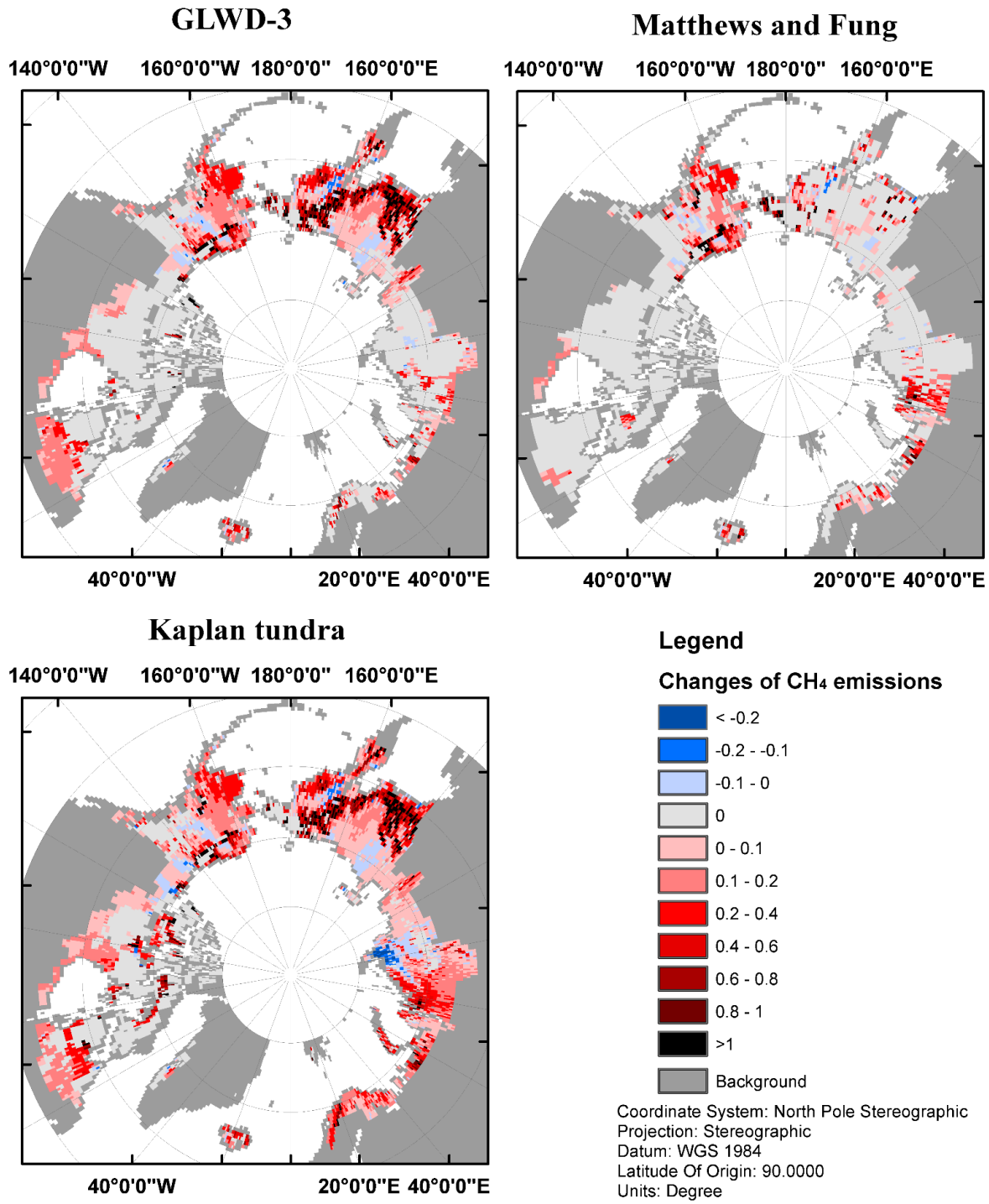

Figure 11. Fractional change in CH_4 emissions in 1991-2009 relative to the standard period (1961-1990), where 0 means no change.

Simulated average annual CH_4 emissions of Arctic tundra (Figure 10) were calculated from the fluxes maps (Figure 9) and the fractional maps (Figure 8). All three maps show that south Alaska, western Siberia, central and eastern Canada annually emitted large amounts of CH_4 during the climate standard period, and also indicate that the largest emissions are all located in eastern Canada, where Lake Manicouagan and Michikamau Lake are located. Comparing the three maps, Kaplan still provides the most complete information in northern Siberia and northern Scandinavia, and Matthews and Fung provides the least, especially missing eastern Siberia and eastern Canada (Figure 10). For eastern Siberia, GLWD-3 clearly shows Verkhoyansk Range and Chersky Range, but Kaplan seems to just indicate Verkhoyansk Range (Figure 10). For the whole Arctic tundra area, simulations using the GLWD-3 map result in 10.13TgC (1.16 gC m^{-2} yr^{-1}) annually emitted as methane to the atmosphere, but the estimates using the other two maps are approximately half this amount (Table 11). Diffusion accounts for most of emissions at nearly 70%. The plant-mediated transport emissions estimated using the three fractional wetland maps account for 30% - 31% of the annual total CH_4 emissions, and ebullition accounts the least (Table 11). Compared with the results of simulations using regional process-based models in the McGuire et al. (2012) study, all estimations using the three fractional wetland maps underestimate annual total CH_4 emissions, which is up to five times less (Table 12). The underestimations also occur when compared with the results of observations in the same study, although the underestimations are not that large (Table 12).

The normalized changes of annual CH_4 emissions between the climate standard period (1961-1990) and the following period (1991-2009) show a general 12% - 13% increase of CH_4 emission over time (Table 11). All three maps indicate that rapid increases happened in northern Alaska (Brooks Range) (Figure 11). Both GLWD-3 and the Kaplan map show very significant increases in eastern Siberia (Kolyma Range and west) (Figure 11). Only the Kaplan map shows that CH_4 emissions from the Barren Grounds, northern Canada, increased; and it also indicates the greatest increases in Scandinavia's emissions compared to the other two maps (Figure 11).

Table 11. Annual mean CH_4-C Exchange

Maps	1961-1990				1991-2009				Total
	Diffusion	Ebullition	Plant	Total	Diffusion	Ebullition	Plant	Total	Changes
Tg C yr^{-1}									
GLWD-3	7.08(69.9%)	0.01(0.1%)	3.04(30.0%)	10.13	7.87(68.8%)	0.02(0.1%)	3.56(31.1%)	11.44	+12.92%
M & F	3.63(69.5%)	0.01(0.2%)	1.58(30.3%)	5.22	4.04(68.5%)	0.01(0.2%)	1.85(31.3%)	5.94	+12.99%
Kaplan 2007	4.08(68.7%)	0.01(0.1%)	1.85(31.2%)	5.94	4.51(67.5%)	0.01(0.1%)	2.17(32.4%)	6.69	+12.66%
g C m^{-2} yr^{-1}									
GLWD-3	0.81(69.9%)	0.00(0.1%)	0.35(30.0%)	1.16	0.90(68.8%)	0.00(0.1%)	0.41(31.1%)	1.31	+12.92%
M & F	0.41(69.5%)	0.00(0.2%)	0.18(30.3%)	0.60	0.46(68.5%)	0.00(0.2%)	0.21(31.3%)	0.67	+12.99%
Kaplan 2007	0.47(68.7%)	0.00(0.1%)	0.21(31.2%)	0.68	0.52(67.5%)	0.00(0.1%)	0.25(32.4%)	0.76	+12.66%

Table 12. Comparison of estimates of annual CH_4 emission among the three fractional wetland maps, observations, and other process-based models.

Maps & other sources	1990-1999		2000-2006		1990-2006	
Tg C yr^{-1}						
GLWD-3[a]	11	(2 to 21)	12	(2 to 23)	11	(2 to 22)
M & F[a]	5	(1 to 11)	6	(1 to 12)	6	(1 to 12)
Kaplan 2007[a]	6	(1 to 12)	7	(1 to 14)	7	(1 to 13)
Observations[b]	10	(-1 to 22)	20	(-11 to 51)	11	(0 to 22)
Regional Process-Based models[c]	25	(15 to 34)	28	(18 to 37)	26	(16 to 35)

[a] The values in brackets are calculated using the parameter sets detected from min/max overall CH_4 fluxes.

[b] 250 estimates from 120 published papers was achieved by using manual chambers, automatic chambers, and eddy covariance techniques (McGuire et al. 2012).

[c] The values were estimated by simulations used LPJ-GUESS WHyMe (2012) and TEM6 (McGuire et al. 2012).

More detailed temporal variations of simulated Arctic tundra annual CH_4 emissions during 1961 to 2009 are shown in Figure 12. Just as the three maps showed very different CH_4 emissions in Table 11, the quantitative temporal differences in CH_4 emissions among three maps are very significant (Figure 12); however, the three maps' CH_4 emissions simulated by the overall best parameter set are in the common area of three maps bias, which was created by simulations using the parameter sets with the maximum and minimum total annual CH_4 emissions at the five observation sites (Figure 12). Thus, the uncertainties arising from differences in the fractional distribution among the three maps are much greater than the uncertainties of the best 12 (top 50% at each site) parameter sets (Figure 12).

In order to detect the dynamic variations of regional CH_4 emissions from Arctic tundra during 1961 to 2009, annual CH_4 emission simulated by each wetland map was normalized by its average CH_4 emission in the climate standard period (Figure 13). Simulations by all three maps likely show the same fluctuation and the same increasing trend, which has highest emissions in 2003 and 2005 and two significantly rapid low ebbs in 1965 and 1992 (Figure 13). The uncertainties arising from dynamic fluctuations for the three maps is smaller than that due to the uncertainty arising from use of the best 12 parameter sets (Figure 13).

For the three pathways of CH_4 emission shown in Figure 14, diffusion emissions have the most similar characteristics to the total emissions. Plant-mediated emissions show the same trend, but their fluctuations are lower in extreme periods and uncertainties due to the 12 best parameter sets are smaller. The trends in ebullition emissions vary greatly and do not correlate with the total emissions, and fluctuations of ebullition seem to be very random, though with very small uncertainties due to the best 12 parameter sets (Figure 14). Figure 15 shows a result of comparison of CH_4 emissions among the three fractional wetland maps in a quantitative way. R^2 shows how coincident the trends of the annual variance of simulated different pathways' CH_4 emissions among three maps are. In general, plant-mediated transport provides the highest coincident variance among the three fractional wetland maps compared with the other transport pathways, and ebullition provides the least. Of the three fractional wetland maps, GLWD-3 and Kaplan 2007 have the highest coincident variance in all transport pathways even in ebullition (Figure 15).

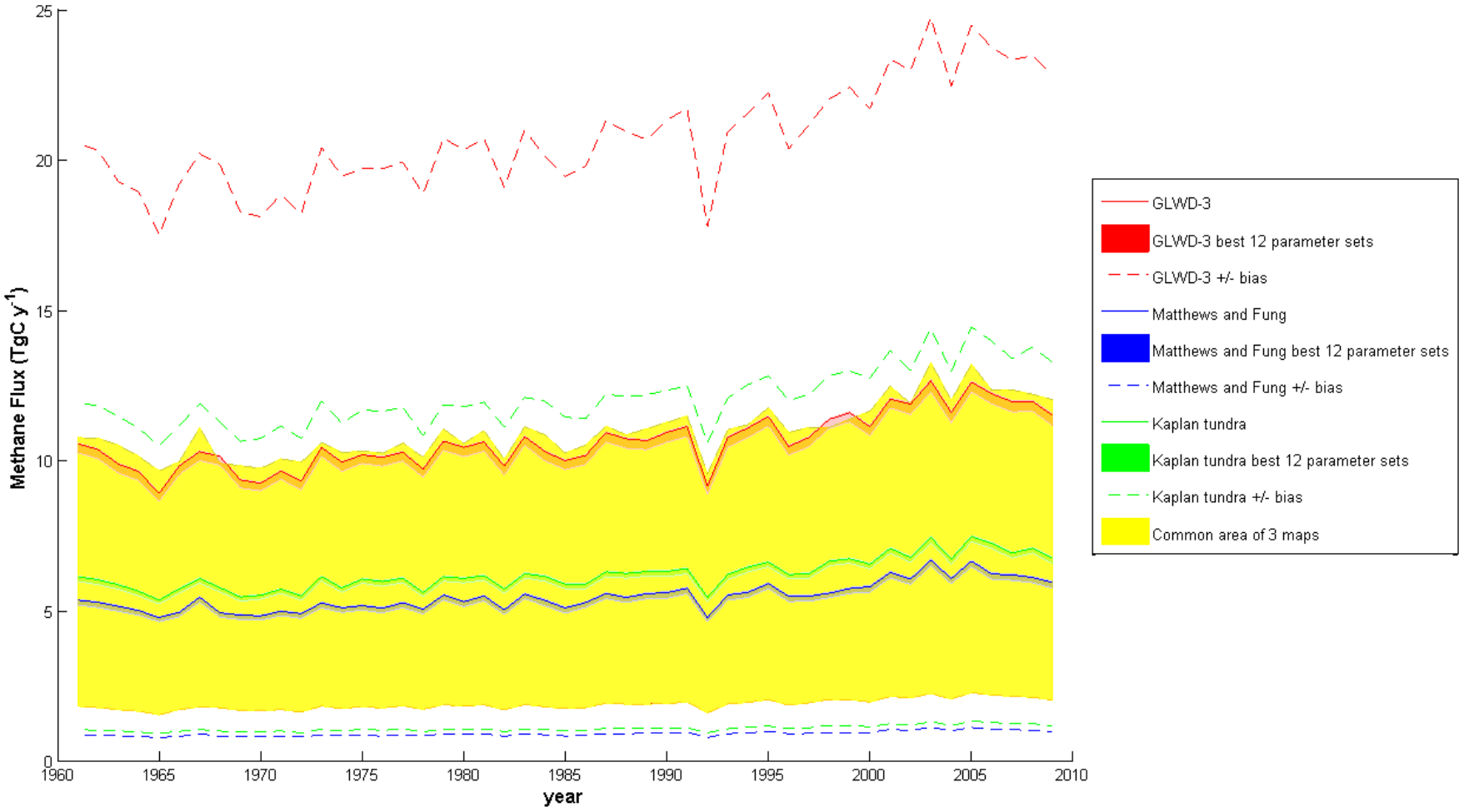

Figure 12. The Arctic tundra annual methane emission (TgC yr^{-1}) determined using the three different wetland fraction maps.

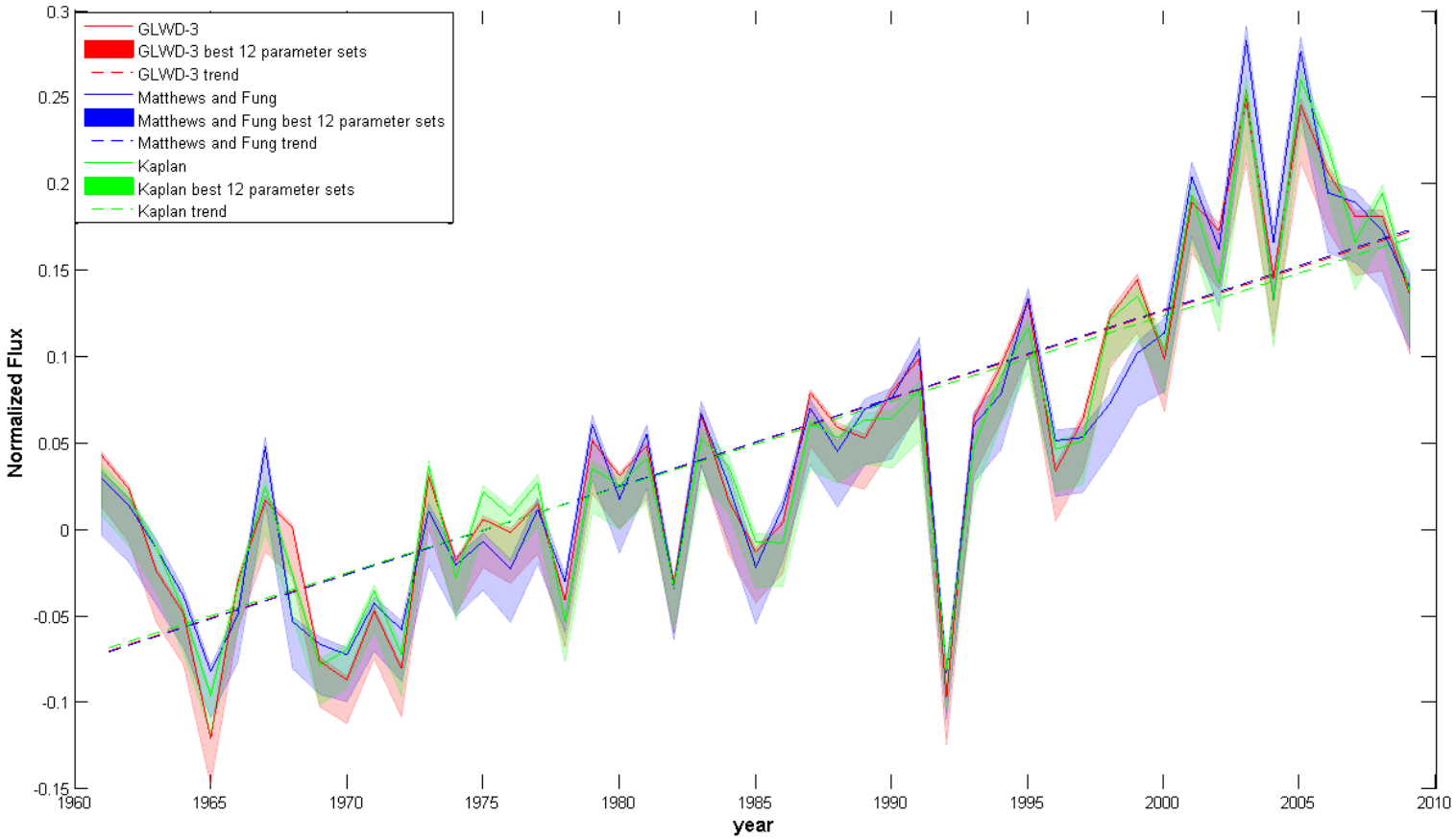

Figure 13. Arctic tundra annual methane emissions normalized to the standard period (1961-1990) for the three wetland fractional maps.

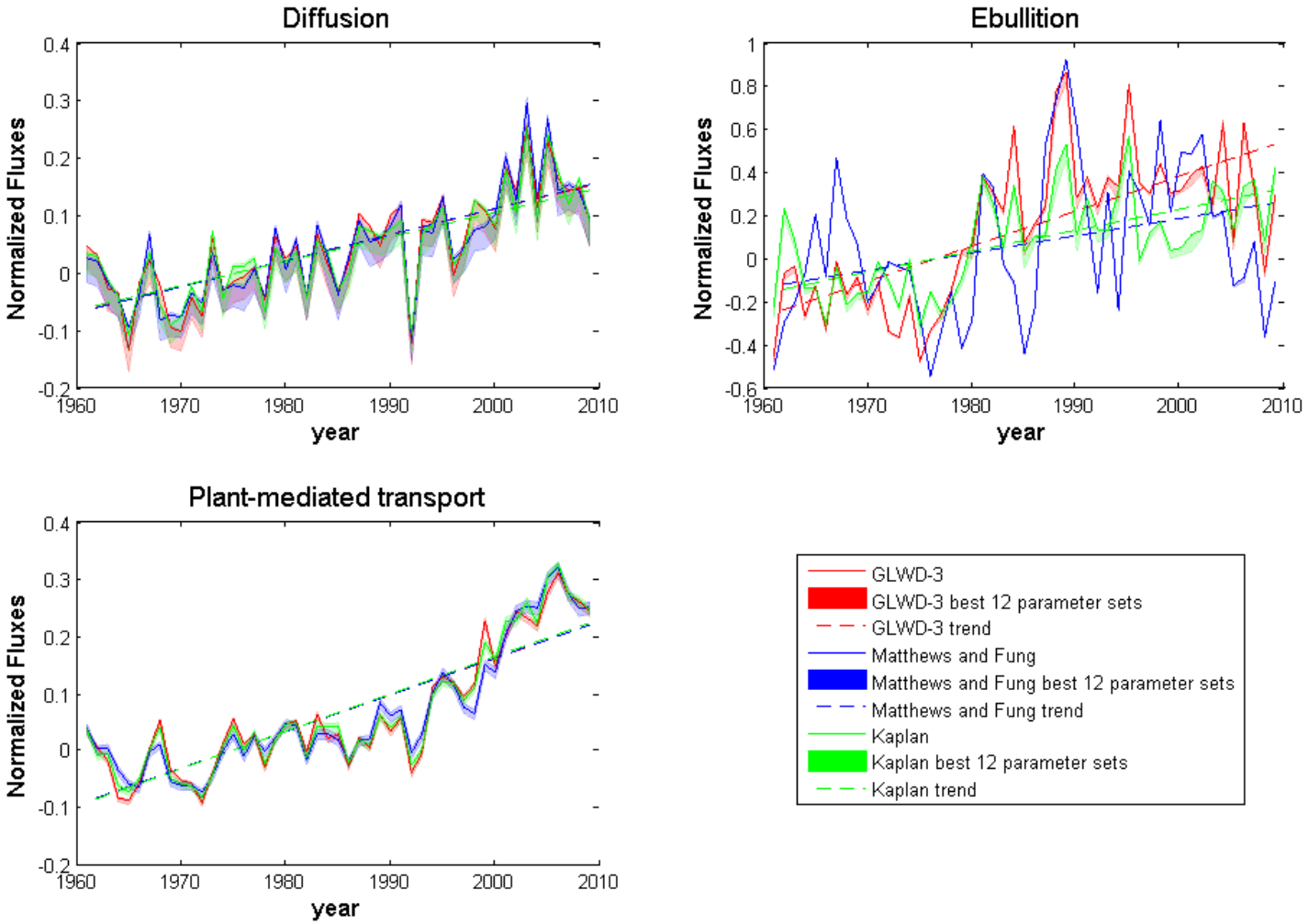

Figure 14. Annual methane fluxes from three pathways normalized to the standard period (1961-1990) in three pathways for the three wetland fractional maps.

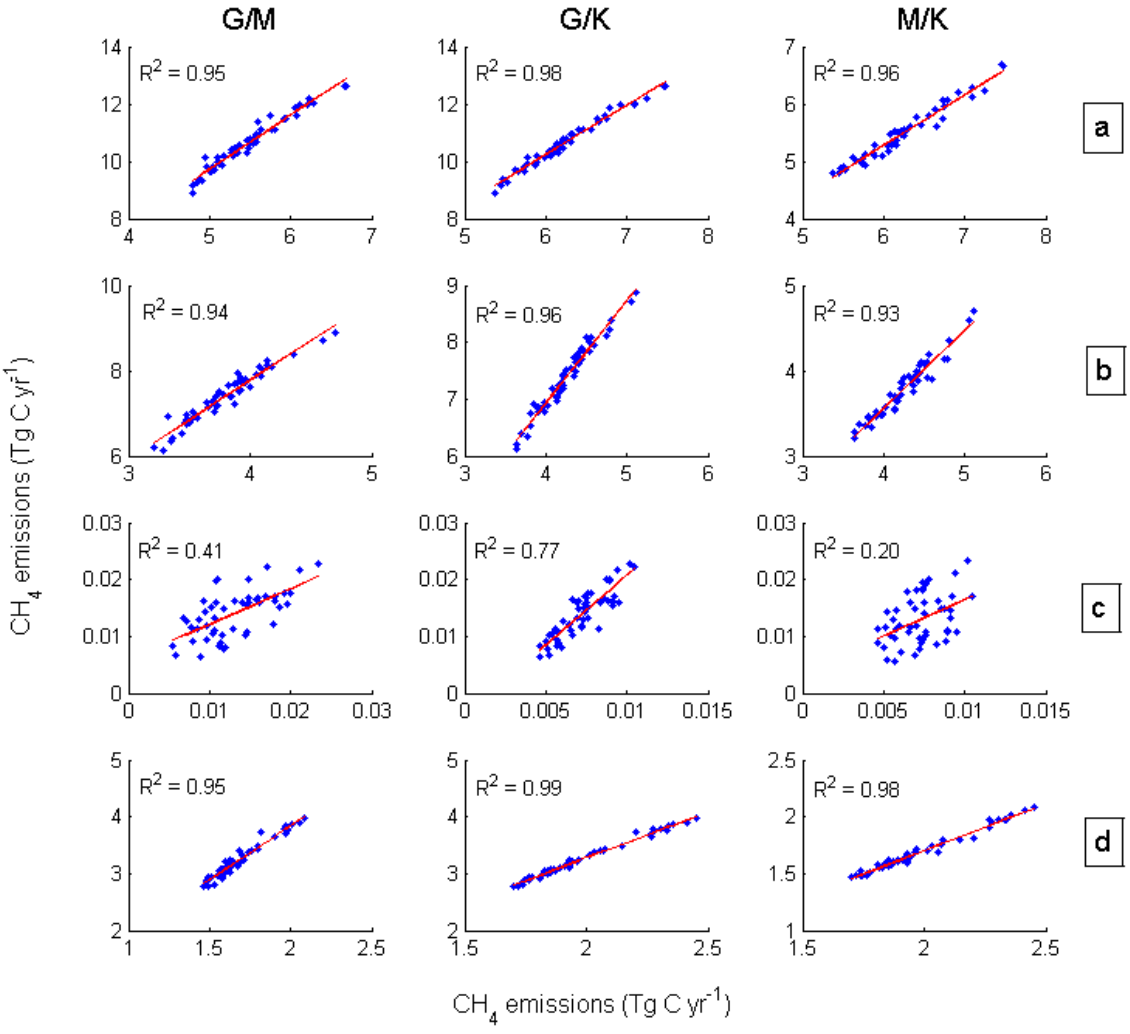

Figure 15. Multiple comparisons of annual CH_4 emissions among the three fractional wetland maps. G: GLWD-3; M: Matthews and Fung; K: Kaplan 2007; a. Total; b. Diffusion; c. Ebullition; d. Plant-mediated transport.

4.4 Interrelationship among output variables (soil temperature, water table position, NPP, and CH_4 fluxes)

Annual NPP is a very important indicator of carbon sequestration by vegetation. In this study, NPP mainly represents net uptake by cool/flood tolerant grass and sphagnum moss PFTs, which are some of the main vegetation types growing in the Arctic tundra wetlands (Table 1). Simulated annual NPP shows a very strong positive correlation with simulated annual average water table position and annual average soil temperature at 25 cm from the model (Figure 16). Comparing with water table position and soil temperature at the first layer (25 cm), NPP has a strong limitation when annual average soil temperature falls below approximately −4 ºC at 25 cm; conversely, significant NPP values always exist when annual average soil temperature at

25 cm is above −4 Cº even if the water table position is very low (Figure 16). Annual CH_4 emissions in Arctic tundra during 1961-2009 also show equally significant relationships to water table position and soil temperature (Figure 17). An annual average soil temperature at 25 cm of −4 ºC is also the threshold value for CH_4 emissions; in other words, there is likely no CH_4 emissions when annual average soil temperature at 25 cm falls below −4 ºC even if water table position is high enough (Figure 17). Similarly, the limitation of annual average water table position to produce methane is about −0.25 m (Figure 17).

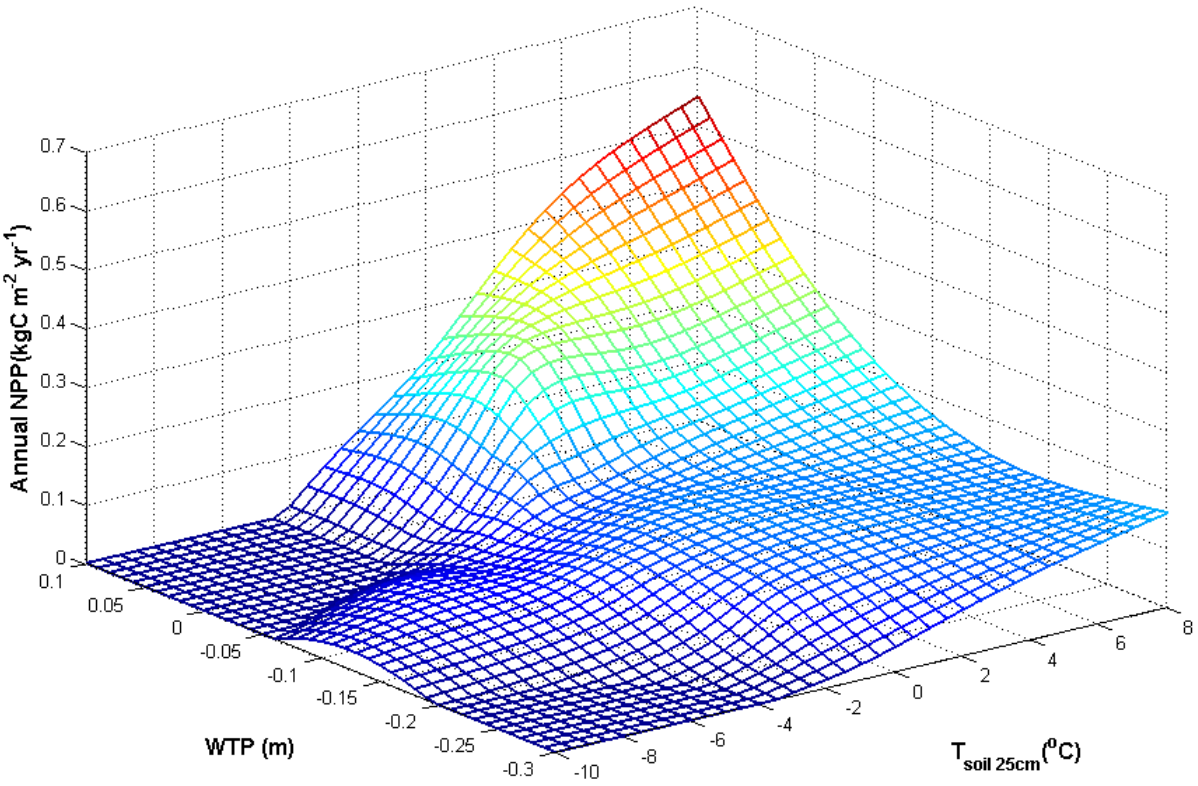

Figure 16. Fitting surface of annual NPP, water table position and soil temperature at 25 cm below the surface in the period 1961-2009.

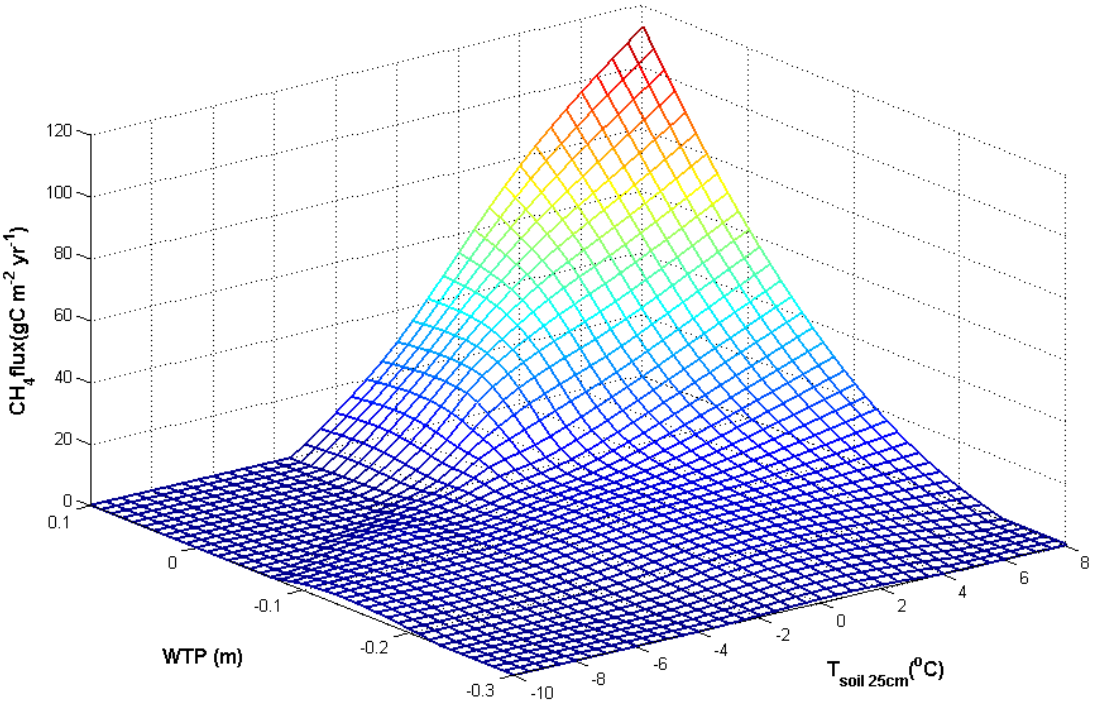

Figure 17. Fitting surface of annual methane fluxes, water table position, and soil temperature at 25 cm below the surface in the period 1961-2009.

In order to analyze seasonal differences, each year in 1961-2009 is separated into four seasons: spring (Mar-May), summer (Jun-Aug), autumn (Sep-Nov), and winter (Dec-Feb). The scatter plots for the four seasons' average daily CH_4 flux represent a general increasing trend along both water table position and the first layer's soil temperature (Figure 18). In the Arctic tundra region, the ranges of annual average water table position in each of the four seasons is similar, ranging between the hydrology submodel's imposed limits of -0.3 m to +0.1 m (Figure 18). In contrast to water table position, annual average soil temperature at 25 cm in the four seasons shows obvious seasonal variances, which are the highest in summer and the lowest in winter (Figure 18). The maximum CH_4 flux of approximately 400mgC m^{-2} d^{-1} occurs in summer at warm, wet sites, and; fluxes in autumn are significantly higher than in spring and winter (Figure 18).

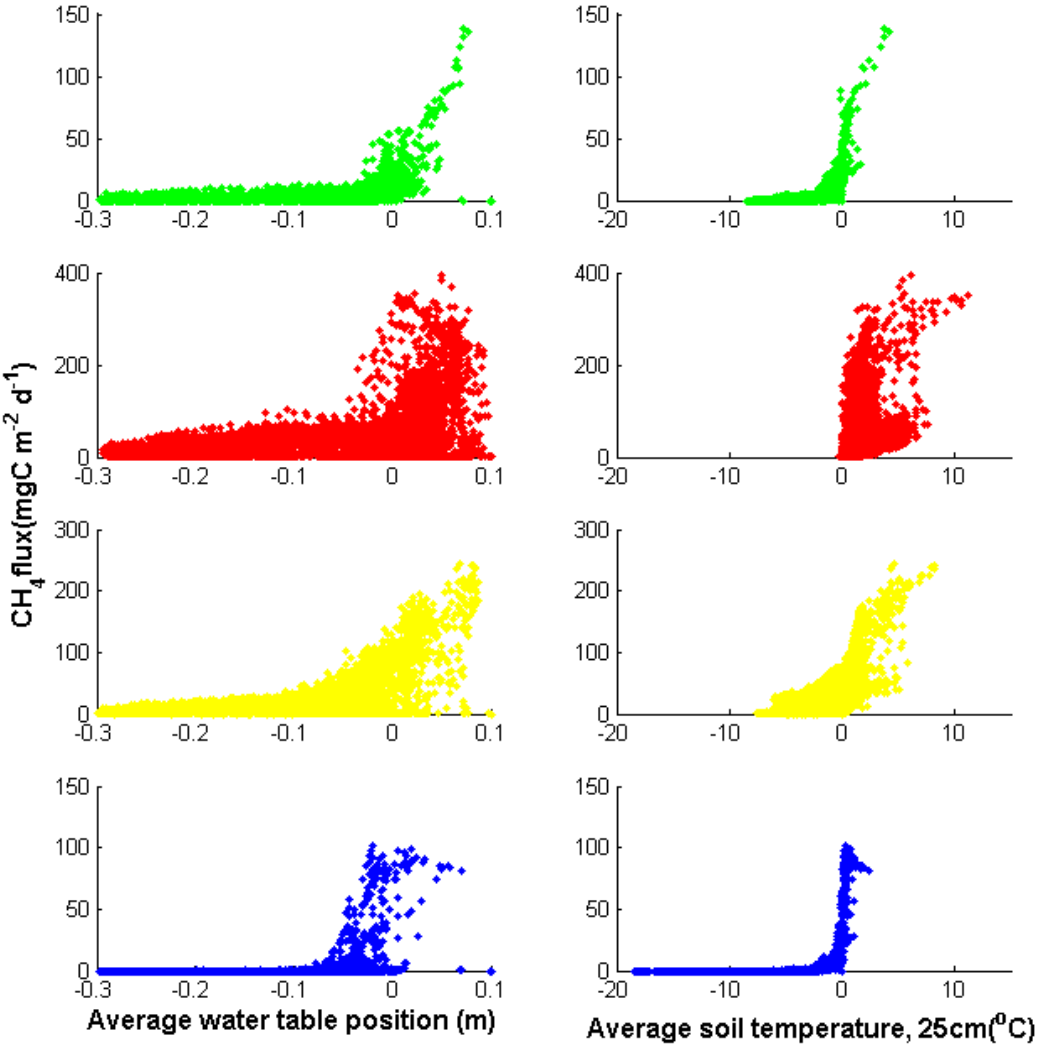

Figure 18. Seasonal average water table position and soil temperature at 25 cm below ground surface vs. log methane fluxes. (spring, summer, autumn, winter)

After fitting a surface on the scatter points in 3D a figure with three variables (CH_4 fluxes, water table position, and soil temperature at 25cm) was created (Figure 19). The seasonal differences are now much clearer; Arctic tundra generally produces larger CH_4 fluxes in autumn than in spring and winter (Figure 18). In addition, the surfaces show that the maximum fluxes at particularly high water table positions and high soil temperature conditions in winter could be larger than from the same conditions in other seasons (Figure 19).

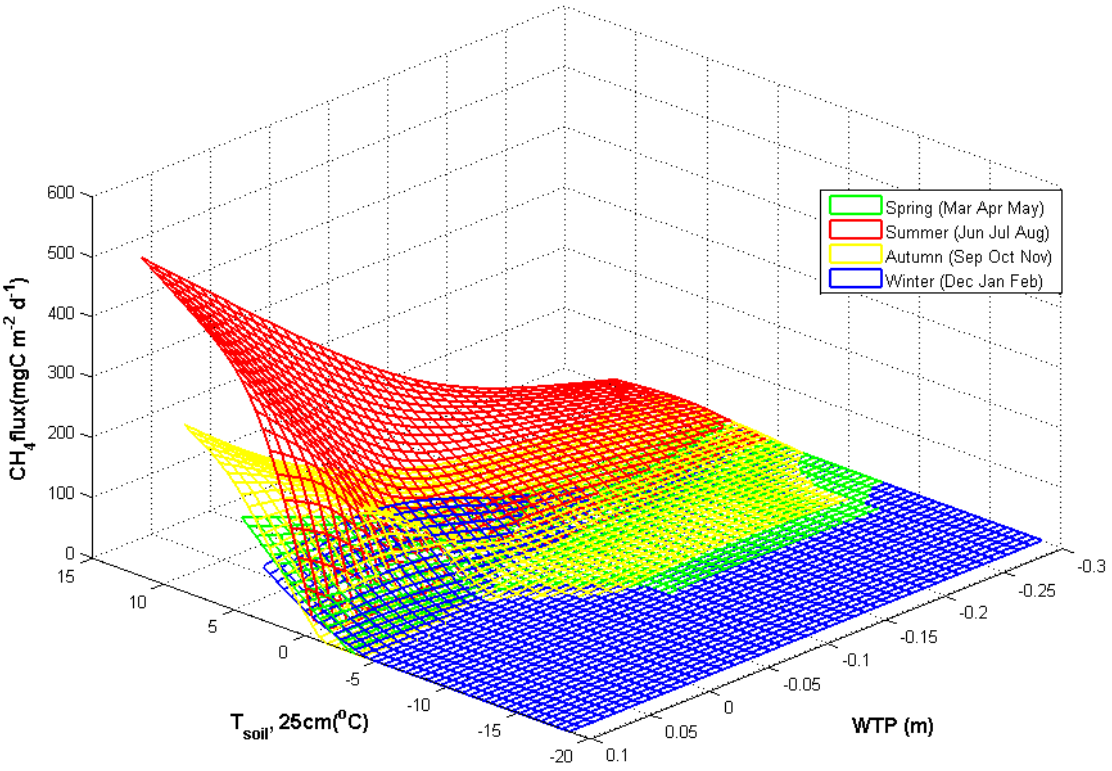

Figure 19. Seasonal average water table position and soil temperature at 25 cm below the surface and daily-averaged methane flux shown in 3D.

Methane fluxes from three transport pathways contribute to the total CH_4 fluxes, with diffusion contributing the most in these model simulations. Along an increasing water table gradient, total fluxes, diffusion fluxes and plant-mediated transport fluxes seem to show an exponential increase above −0.1m (Figure 20). However, total fluxes, diffusion fluxes and plant-mediated transport fluxes show a linear change when soil temperature at 25 cm increases below 0 °C (Figure 20). Around 0 °C at 25 cm below the surface, there seems to be a jump. The 'jump' of total fluxes and diffusion fluxes are similar, but that of plant-mediated transport fluxes are much more rapid (Figure 20). Ebullition fluxes contribute the least and appear to represent a random distribution along a limited range of water table position and first layer soil temperature (Figure 20). A surface on 3D scatter points of the three transport pathways for CH_4 fluxes, water table position and soil temperature at 25 cm, resulted in the clearer quantitative relationship shown in Figure 21.

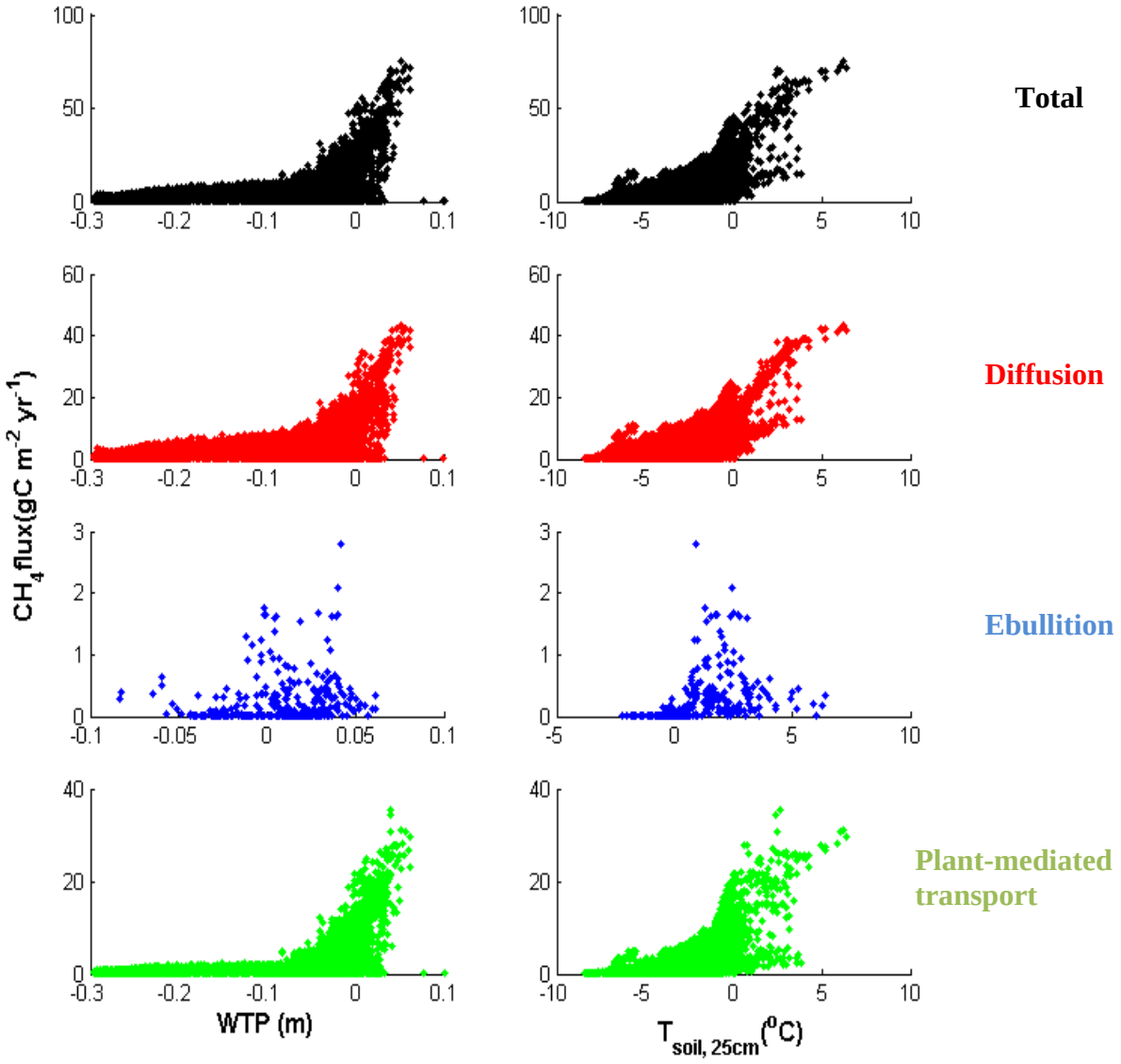

Figure 20. Annual average water table position and soil temperature at 25cm below the surface vs. annual methane flux.

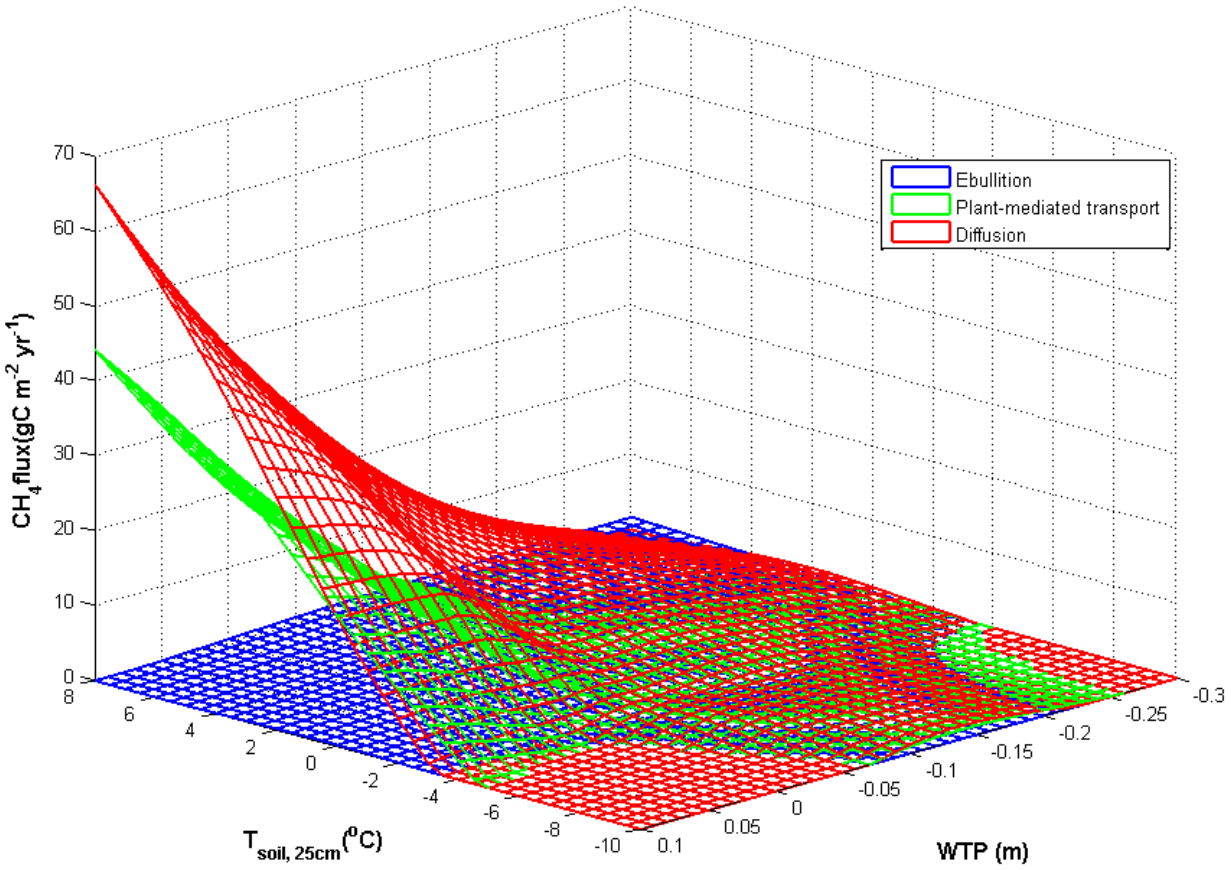

Figure 21. Annual average water table position and soil temperature at 25 cm below the surface and annual methane flux per pathway, shown in 3D.

5 Discussion

For the first time, LPJ-GUESS WHyMe has been used to estimate CH_4 emissions from Arctic tundra wetlands during the period of 1961-2009 according to multisource fractional wetland maps: GLWD-3, Matthews and Fung, and Kaplan 2007.

Five parameters in the model were tested for sensitivity and optimized before the model was applied to simulate Arctic tundra CH_4 emissions. CH_4/CO_2 and f_{oxid} were found to be the most important parameters influencing total CH_4 fluxes in LPJ-GUESS WHyMe, similar to the findings of the Wania et al. (2010) study with LPJ-WHyMe. The signs of the RPCC values of these two important parameters also agree with the signs shown in Wania et al. (2012). The importance of f_{oxid} has a slight change with changing of time at BOREAS, but in general, the

spatial variances of the importance of parameters were more significant than the temporal variance (Table 5). This indicates that these parameters should be optimized when applying the model to local or regional simulations. However, the signs of the RPCC values of other three parameters were not totally in agreement with the signs shown in Wania et al. (2010). For example, the RPCC value for Rmoist in this study varies from positive (Sallmisuo, Degerö, Abisko) to negative (Minnesota, BOREAS), but Wania et al. (2010) find that it is always positive. For parameter optimization, our new method can confidently investigate a best overall parameter set that, at the same time, is the best site parameter set in a certain range (manually set to 50% in this study), but it's obvious that the best overall parameter set cannot simulate a minimum overall error with respect to observations at each site (Table 7). In addition, it should be noted that the available sites of observations had a very limited representativeness of Arctic tundra due to only one site (Abisko) being situated in the study area. Comparing the best site parameters at Abisko with the overall best parameter set (Table 6), the parameters $CH4/CO_2$ and f_{oxid}, which most influence CH_4 fluxes in the model, were lower and higher respectively, which is likely one of the reasons behind our estimation of total CH_4 fluxes from Arctic tundra being lower than previous published estimates (Table 12). The site simulations based on the best overall parameter set were located in the middle of the range of all simulations based on all testing parameter sets, which indicates that the ranges of parameters were reasonable although they were manually set (Table 3). The difference in total annual CH_4 fluxes with the estimations in the Wania et al. (2010) study cannot only be explained as the result of difference in parameter sets, but it can also be considered a result of difference in model structure, i.e. the difference between a 'gap model' and a DGVM (Table 8). For the site simulations of three transport pathways, the sites which had the most plant-mediated transport fluxes also had the most WetGRS PFT annual NPP. It corresponds with the fact that only WetGRS PFT can transport CH_4 (Frenzel & Rudolph 1998; Colmer 2003; Wania et al. 2009b). However, Table 9 shows WetGRS PFT annual NPP is 0 or below in BOREAS, Degerö, and Abisko, which disagrees with the observation shown in Table 1. This is likely due to the fact that LPJ-GUESS WHyMe was not run separately for the microtopographical features seen in these wetlands, such as hummocks and hollows. Ebullition contributed the least CH_4 fluxes, which agreed with the results in the Wania et al. (2010) study. The limited contribution of ebullition to total CH_4 fluxes was associated with uncertainty and a very variable importance of parameters for ebullition, probably due to its complexity as a process (Tokida et al. 2007) (Figure 6, Table 8, Table 9). In contrast, diffusion contributed the most CH_4 fluxes and determined the peaks of total CH_4 fluxes, but it has been shown using both model simulation and experiment that it is

typically lower than plant-mediated transport (Bhullar et al. 2013; Wania et al. 2010). In this thesis, it can be not identified if the difference was caused by overestimating diffusion or underestimating plant-mediated transport. In LPJ-GUESS WHyMe, the process of CH_4 diffusion depends on a number of experimental formulas based on temperature, amounts of water and air in the soil and the soil porosity (Broecker & Peng 1974; Iiyama & Hasegawa 2005; Wania et al. 2010), and the process of CH_4 plant-mediated transport depends on simulations of WetGRS PFT (Wania et al. 2010). Therefore, the balance between diffusion and plant-mediated transport could be a result of temperature, hydrology or performance in simulating WetGRS PFT, and work for a further study.

The fractional wetland map is a significant influence on the quantitative estimation of regional CH_4 emissions. The area of the Arctic tundra wetlands estimated from GLWD-3 was almost twice as large as the area estimated from Matthews & Fung and Kaplan 2007, and it seems to directly scale the Arctic tundra wetland CH_4 emissions estimated from GLWD-3, which were also almost twice as much as from the other two maps (Table 10, Table 11). Furthermore, these large estimated CH_4 emissions from GLWD-3 already touched the upper limit of estimated CH_4 emissions from Matthews & Fung (Figure 12); therefore, the uncertainty of estimating regional CH_4 emissions from the difference between GLWD-3 and the other two maps is much larger than from parameter sets. However, all regional simulations of CH_4 emissions from three fractional wetland maps were underestimated comparing with the McGuire et al. (2012) paper. It is likely that one reason for these underestimates was parameter optimization. For three transport pathways, the model estimated about 31% of total Arctic tundra wetland CH_4 emitted by plant-mediated transport that was well-match to the site simulation at Abisko (29.0%) (Table 8), which was the only observation in Arctic tundra.

In contrast to the differences seen in the quantitative estimation of total Arctic tundra CH_4 emissions, fractional wetland maps showed a similar dynamically annual variation of Arctic tundra wetland CH_4 emissions. The two obvious troughs in 1965 and 1992 could mainly have been forced by drops of atmospheric temperature due to the Mount Agung volcano eruption in 1963 and the Mount Pinatubo volcano eruption in 1991 (Mass & Portman 1989; Lucht et al. 2002). The uncertainty of total annual CH_4 emissions simulated by the best 12 parameter sets, which have the only differences in f_{oxid} and k_{exu}^{10}, result mainly from the uncertainty of annual diffusion emissions, and probably can be explained as the result of variations in f_{oxid}, which was identified as the second most influential parameter on diffusion in Abisko. The CH_4 emitted by plant-mediated transport was also significantly influenced by f_{oxid}, which played the

second most important role following CH_4/CO_2, but its uncertainty was not as large as diffusion's (Table 5, Figure 13, and Figure 14). The extremely strong correlation in plant-mediated transport among the three fractional wetland maps indicated that the temporal variances of plant-mediated transport are more coincident than that of the other transport pathways (Figure 15). In other words, diffusion and ebullition have more significant influence from spatial variances in Arctic tundra.

For the detailed analysis of water table position and soil temperature, since WetGRS is the dominant PFT when the water table position is above the surface (over 0 m) and its low temperature limit and lower range of temperature for photosynthesis are −5°C and +5°C, the average annual NPP sharply decreased from +5°C to −5°C of soil temperature at 25 cm when the water table position is over 0 m (Figure 16). The annual NPP had a significant buffer when the water table position is at 0 m because the PFT 'pmoss' starts to grow. When the water table position is below −0.05m, the surface slope becomes gentler because the proportions of 'WetGRS' and 'pmoss' are almost in equilibrium (Figure 16). The sharpest rise, which is located around −0.2 to −0.05 m of water table position and below -5°C of soil temperature at 25 cm, is caused by uncertainties in surface fitting (Figure 16). In addition, since only 'WetGRS' can be a plant-pathway for transport of CH_4 (Frenzel & Rudolph 1998; Colmer 2003; Wania et al. 2009b), the plant-mediated transport surface in Figure 21 can represent the relationship among the annual NPP of 'WetGRS', the water table position and the soil temperature at 25 cm. Therefore, the significant plant-mediated transport when the water table position is located between −0.1 to 0.1 m indicates that 'WetGRS' prefers to grow when the water table position lies in this range (Figure 20). The wide range of annual CH_4 fluxes transported through plant, as well as ebullition but not diffusion, at the soil temperature of 0°C is probably due to the fact that ice melting can lead to thicker activity in soil layers, form where CH_4 can be directly emitted to the atmosphere through aerenchyma (Figure 20). Ebullition only exist above 0 value of both water table position and soil temperature because of the several interacting model processes: bubble formation below the water table only, the bubbled methane into the first unsaturated layer if the water table is below the surface, and bubble formation if the soil temperature above 0°C (Figure 20). The fitting surface among total annual CH_4 fluxes, water table position, and soil temperature also presents the combined characteristics of the each pathway's surface and it shows annual CH_4 fluxes are more sensitive to variability in soil temperature when the water table is above the surface, which is as same as the findings in the Olefeldt et al. (2013) study. For the seasonal analysis, in spring and autumn, the same situations

with plant-mediated transport that a wide range of annual CH_4 fluxes exist when the soil temperature at 25 cm is 0°C (Figure 18). It can be identified that it is directly caused by plant-mediated transport and water table position. However, the relationship between the CH_4 fluxes and the water table position, which is nearly an exponential trend, does not present significant seasonal changes (Figure 18).

6 Conclusion

In this research, LPJ-GUESS WHyMe was used to estimate CH_4 emissions from Arctic tundra wetlands using three different fractional wetland maps. The three fractional wetland maps led to significant differences in estimation of Arctic tundra CH_4 emissions. The uncertainties of CH_4 emissions in Arctic tundra caused by fractional wetland maps are larger than that those caused by parameter uncertainty. However, the temporal variability of CH_4 emissions in Arctic tundra is not significantly different when using different fractional wetland maps. Diffusion has been detected as the dominant process for methane transport from wetland to the atmosphere in Arctic tundra. Soil temperature at 25 cm is more influential for CH_4 fluxes in Arctic tundra if the water table position is above the soil surface. In addition, plant-mediated transport contributes the most particular characteristics when the soil temperature at 25 cm is around 0°C in spring and summer. In future research, the model, LPJ-GUESS WHyMe can be used to simulate CH_4 emissions in future scenarios. Our results indicate that it would be a significant improvement if it also contained a model that simulates dynamic wetland fraction based on topography and driven by climate.

7 Reference

Bergamaschi, P., C. Frankenberg, J. F. Meirink, M. Krol, F. Dentener, T. Wagner, U. Platt, J. O. Kaplan, S. Korner, M. Heimann, E. J. Dlugokencky & A. Goede (2007) Satellite chartography of atmospheric methane from SCIAMACHY on board ENVISAT: 2. Evaluation based on inverse model simulations. *Journal of Geophysical Research-Atmospheres,* 112.

Bhullar, G. S., P. J. Edwards & H. O. Venterink (2013) Variation in the plant-mediated methane transport and its importance for methane emission from intact wetland peat mesocosms. *Journal of Plant Ecology,* 6**,** 298-304.

Birkett, C. M. & I. M. Mason (1995) A new global lakes database for a remote-sensing program studying climatically sensitive large lakes. *Journal of Great Lakes Research,* 21**,** 307-318.

Broecker, W. S. & T. H. Peng (1974) Gas exchange rates between air and sea1. *Tellus,* 26**,** 21-35.

Bubier, J. L., Crill, P. M., Varner, R. K., and Moore, T. R.: BOREAS TGB-01/TGB-03 CH4 chamber flux data: NSA Fen. Data set. Available online [http://www.daac.ornl.gov] from Oak Ridge National Laboratory Distributed Archive Center, Tech. rep., Oak Ridge, Tennessee, USA, 1998.

Cao, M. K., S. Marshall & K. Gregson (1996) Global carbon exchange and methane emissions from natural wetlands: Application of a process-based model. *Journal of Geophysical Research-Atmospheres,* 101**,** 14399-14414.

Ciais, P., C. Sabine, G. Bala, L. Bopp, V. Brovkin, J. Canadell, A. Chhabra, R. DeFries, J. Galloway, M. Heimann, C. Jones, C. Le Quéré, R.B. Myneni, S. Piao and P. Thornton, 2013: Carbon and Other Biogeochemical Cycles. In: Climate Change 2013: The Physical Science Basis. Contribution of Working Group I to the Fifth Assessment Report of the Intergovernmental Panel on Climate Change [Stocker, T.F., D. Qin, G.-K. Plattner, M. Tignor, S.K. Allen, J. Boschung, A. Nauels, Y. Xia, V. Bex and P.M. Midgley (eds.)]. Cambridge University Press, Cambridge, United Kingdom and New York, NY, USA.

Colmer, T. D. (2003) Long-distance transport of gases in plants: a perspective on internal aeration and radial oxygen loss from roots. *Plant Cell and Environment,* 26**,** 17-36.

Dise, N. B. (1993) Methane emission from minnesota peatlands - spatial and seasonal variability. *Global Biogeochemical Cycles,* 7**,** 123-142.

Dlugokencky, E. J., E. G. Nisbet, R. Fisher & D. Lowry (2011) Global atmospheric methane: budget, changes and dangers. *Philosophical Transactions of the Royal Society a-Mathematical Physical and Engineering Sciences,* 369**,** 2058-2072.

Dugan, P. (Ed.), 1993. Wetlands in Danger: A World Conservation Atlas, In Association with IUCN: The World Conservation Union, Oxford University Press, New York.

ESRI: Environmental Systems Research Institute, 1992. ArcWorld 1:3 Mio. Continental Coverage. Redlands, CA. Data obtained on CD.

ESRI: Environmental Systems Research Institute, 1993. Digital Chart of the World 1:1 Mio. Redlands, CA. Data obtained on 4 CDs (also available online at http://www.maproom.psu.edu/dcw/).

European Topic Centre on Terrestrial Environment (ETCTE) (2000),Corine land cover database (Version 12/2000 extended coverage), Eur. Environ. Agency, Copenhagen. (Available at http://dataservice.eea.eu.int/dataservice/metadetails.asp?id=571).

Frenzel, P. & J. Rudolph (1998) Methane emission from a wetland plant: the role of CH4 oxidation in Eriophorum. *Plant and Soil,* 202**,** 27-32.

Gedney, N., P. M. Cox & C. Huntingford (2004) Climate feedback from wetland methane emissions. *Geophysical Research Letters,* 31**,** L20503.

Gerten, D., S. Schaphoff, U. Haberlandt, W. Lucht & S. Sitch (2004) Terrestrial vegetation and water balance - hydrological evaluation of a dynamic global vegetation model. *Journal of Hydrology,* 286**,** 249-270.

Granberg, G., M. Ottosson-Lofvenius, H. Grip, I. Sundh & M. Nilsson (2001) Effect of climatic variability from 1980 to 1997 on simulated methane emission from a boreal mixed mire in northern Sweden. *Global Biogeochemical Cycles,* 15**,** 977-991.

Hargreaves, K. J. & D. Fowler (1998) Quantifying the effects of water table and soil temperature on the emission of methane from peat wetland at the field scale. *Atmospheric Environment,* 32**,** 3275-3282.

Hartmann, D.L., A.M.G. Klein Tank, M. Rusticucci, L.V. Alexander, S. Brönnimann, Y. Charabi, F.J. Dentener, E.J. Dlugokencky, D.R. Easterling, A. Kaplan, B.J. Soden, P.W. Thorne, M. Wild and P.M. Zhai, 2013: Observations: Atmosphere and Surface. In: Climate Change 2013: The Physical Science Basis. Contribution of Working Group I to the Fifth Assessment Report of the Intergovernmental Panel on Climate Change [Stocker, T.F., D. Qin, G.-K. Plattner, M. Tignor, S.K. Allen, J. Boschung, A. Nauels, Y. Xia, V. Bex and P.M. Midgley (eds.)]. Cambridge University Press, Cambridge, United Kingdom and New York, NY, USA.

Harris, I., P. D. Jones, T. J. Osborn & D. H. Lister (2013) Updated high-resolution grids of monthly climatic observations – the CRU TS3.10 Dataset. *International Journal of Climatology*.

Helton, J.C. and Davis, F.J. (2000). Sampling-based methods. In: Saltelli, A., Chan, K., and Scott, E.M., editors, Sensitvity Analysis, Wiley Series in Probability and Statistics, pages 101-153. John Wiley & Sons, ltd., Chichester, New York, USA.

Hely, C., L. Bremond, S. Alleaume, B. Smith, M. T. Sykes & J. Guiot (2006) Sensitivity of African biomes to changes in the precipitation regime. *Global Ecology and Biogeography,* 15**,** 258-270.

Hodson, E. L., B. Poulter, N. E. Zimmermann, C. Prigent & J. O. Kaplan (2011) The El Nino-Southern Oscillation and wetland methane interannual variability. *Geophysical Research Letters*, 38.

ICOLD: International Commission on Large Dams, 1984. Word Register of Dams. 1984 Full Edition and 1988 Updating, ICOLD, Paris.

ICOLD: International Commission on Large Dams, 1998. Word Register of Dams. 1998 book and CD-ROM, ICOLD, Paris.

Iiyama, I. & S. Hasegawa (2005) Gas Diffusion Coefficient of Undisturbed Peat Soils. *Soil Science & Plant Nutrition,* 51**,** 431-435.

Jackowicz-Korczynski, M., T. R. Christensen, K. Backstrand, P. Crill, T. Friborg, M. Mastepanov & L. Strom (2010) Annual cycle of methane emission from a subarctic peatland. *Journal of Geophysical Research-Biogeosciences,* 115.

Joint Research Centre (JRC) (2003), Global Land Cover 2000 database, Eur. Comm., Ispra, Italy. (Available at http://www.gvm.jrc.it/glc2000).

Kirschke, S., P. Bousquet, P. Ciais, M. Saunois, J. G. Canadell, E. J. Dlugokencky, P. Bergamaschi, D. Bergmann, D. R. Blake, L. Bruhwiler, P. Cameron-Smith, S. Castaldi, F. Chevallier, L. Feng, A. Fraser, M. Heimann, E. L. Hodson, S. Houweling, B. Josse, P. J. Fraser, P. B. Krummel, J. F. Lamarque, R. L. Langenfelds, C. Le Quere, V. Naik, S. O'Doherty, P. I. Palmer, I. Pison, D. Plummer, B. Poulter, R. G. Prinn, M. Rigby, B. Ringeval, M. Santini, M. Schmidt, D. T. Shindell, I. J. Simpson, R. Spahni, L. P. Steele, S. A. Strode, K. Sudo, S. Szopa, G. R. van der Werf, A. Voulgarakis, M. van Weele, R.

F. Weiss, J. E. Williams & G. Zeng (2013) Three decades of global methane sources and sinks. *Nature Geoscience,* 6**,** 813-823.

Lehner, B. & P. Döll (2004) Development and validation of a global database of lakes, reservoirs and wetlands. *Journal of Hydrology,* 296**,** 1-22.

Lehner, B., and P. Döll (2001), WELAREM1: A global wetlands, lakes and reservoirs data set, Univ. of Kassel, Kassel, Germany. (Available at http://www.usf.uni-kassel.de/usf/archiv/daten/lake.en.htm).

Loveland, T.R., Merchant, J.W., Ohlen, D.O., Brown, J.F., 1991. Development of a land-cover characteristics database for the conterminous U.S. Photogramm. Eng. Remote Sensing 57(11), 1453–1463.

Loveland, T.R., Reed, B.C., Brown, J.F., Ohlen, D.O., Zhu, J., Yang, L., Merchant, J.W., 2000. Development of a global land cover characteristics database and IGBP DISCover from 1-km AVHRR data. Int. J. Remote Sensing 21(6/7), 1303–1330.Data and documentation available online at http://edcdaac.usgs.gov/glcc/glcc.html.

Lucht, W., I. C. Prentice, R. B. Myneni, S. Sitch, P. Friedlingstein, W. Cramer, P. Bousquet, W. Buermann & B. Smith (2002) Climatic control of the high-latitude vegetation greening trend and Pinatubo effect. *Science,* 296**,** 1687-1689.

Mass, C. F. & D. A. Portman (1989) Major Volcanic Eruptions and Climate: A Critical Evaluation. *Journal of Climate,* 2**,** 566-593.

Matthews, E. (1983) GLOBAL VEGETATION AND LAND-USE - NEW HIGH-RESOLUTION DATA-BASES FOR CLIMATE STUDIES. *Journal of Climate and Applied Meteorology,* 22**,** 474-487.

Matthews, E. & I. Fung (1987) Methane emission from natural wetlands: Global distribution, area, and environmental characteristics of sources. *Global Biogeochemical Cycles,* 1**,** 61-86.

McGuire, A. D., T. R. Christensen, D. Hayes, A. Heroult, E. Euskirchen, J. S. Kimball, C. Koven, P. Lafleur, P. A. Miller, W. Oechel, P. Peylin, M. Williams & Y. Yi (2012) An assessment of the carbon balance of Arctic tundra: comparisons among observations, process models, and atmospheric inversions. *Biogeosciences,* 9**,** 3185-3204.

McGuire, A. D., S. Sitch, J. S. Clein, R. Dargaville, G. Esser, J. Foley, M. Heimann, F. Joos, J. Kaplan, D. W. Kicklighter, R. A. Meier, J. M. Melillo, B. Moore, I. C. Prentice, N. Ramankutty, T. Reichenau, A. Schloss, H. Tian, L. J. Williams & U. Wittenberg (2001) Carbon balance of the terrestrial biosphere in the twentieth century: Analyses of CO2, climate and land use effects with four process-based ecosystem models. *Global Biogeochemical Cycles,* 15**,** 183-206.

Mitchell, T. D. & P. D. Jones (2005) An improved method of constructing a database of monthly climate observations and associated high-resolution grids. *International Journal of Climatology,* 25**,** 693-712.

Moore, T. R. & N. T. Roulet (1993) Methane flux: Water table relations in northern wetlands. *Geophysical Research Letters,* 20**,** 587-590.

Myhre, G., D. Shindell, F.-M. Bréon, W. Collins, J. Fuglestvedt, J. Huang, D. Koch, J.-F. Lamarque, D. Lee, B. Mendoza, T. Nakajima, A. Robock, G. Stephens, T. Takemura and H. Zhang, 2013: Anthropogenic and Natural Radiative Forcing. In: Climate Change 2013: The Physical Science Basis. Contribution of Working Group I to the Fifth Assessment Report of the Intergovernmental Panel on Climate Change [Stocker, T.F., D. Qin, G.-K. Plattner, M. Tignor, S.K. Allen, J. Boschung, A. Nauels, Y. Xia, V. Bex and P.M. Midgley (eds.)]. Cambridge University Press, Cambridge, United Kingdom and New York, NY, USA.

Olefeldt, D., M. R. Turetsky, P. M. Crill & A. D. McGuire (2013) Environmental and physical controls on northern terrestrial methane emissions across permafrost zones. *Glob Chang Biol,* 19**,** 589-603.

Ringeval, B., P. Friedlingstein, C. Koven, P. Ciais, N. de Noblet-Ducoudre, B. Decharme & P. Cadule (2011) Climate-CH4 feedback from wetlands and its interaction with the climate-CO2 feedback. *Biogeosciences,* 8**,** 2137-2157.

Sitch, S., B. Smith, I. C. Prentice, A. Arneth, A. Bondeau, W. Cramer, J. O. Kaplan, S. Levis, W. Lucht, M. T. Sykes, K. Thonicke & S. Venevsky (2003) Evaluation of ecosystem dynamics, plant geography and terrestrial carbon cycling in the LPJ dynamic global vegetation model. *Glob Chang Biol,* 9**,** 161-185.

Smith, B., I. C. Prentice & M. T. Sykes (2001) Representation of vegetation dynamics in the modelling of terrestrial ecosystems: comparing two contrasting approaches within European climate space. *Global Ecology and Biogeography,* 10**,** 621-637.

Spahni, R., R. Wania, L. Neef, M. van Weele, I. Pison, P. Bousquet, C. Frankenberg, P. N. Foster, F. Joos, I. C. Prentice & P. van Velthoven (2011) Constraining global methane emissions and uptake by ecosystems. *Biogeosciences,* 8**,** 1643-1665.

Tarnocai, C., I. M. Kettles, and B. Lacelle (2000), Peatlands of Canada Database, Open File Rep. 3834, Geol. Surv. of Can., Ottawa, Ont., Canada.

Thoning, K. W., D. R. Kitzis & A. Crotwell. 2013. Atmospheric Carbon Dioxide Dry Air Mole Fractions from quasi-continuous measurements at Barrow, Alaska; Mauna Loa, Hawaii; American Samoa; and South Pole, 1973-2012.

Tokida, T., T. Miyazaki, M. Mizoguchi, O. Nagata, F. Takakai, A. Kagemoto & R. Hatano (2007) Falling atmospheric pressure as a trigger for methane ebullition from peatland. *Global Biogeochemical Cycles,* 21.

Vogelmann, J. E., S. M. Howard, L. M. Yang, C. R. Larson, B. K. Wylie & N. Van Driel (2001) Completion of the 1990s National Land Cover Data set for the conterminous United States from Landsat Thematic Mapper data and Ancillary data sources. *Photogrammetric Engineering and Remote Sensing,* 67**,** 650-652.

Vorosmarty, C. J., K. P. Sharma, B. M. Fekete, A. H. Copeland, J. Holden, J. Marble & J. A. Lough (1997) The storage and aging of continental runoff in large reservoir systems of the world. *Ambio,* 26**,** 210-219.

Walter, B. P. & M. Heimann (2000) A process-based, climate-sensitive model to derive methane emissions from natural wetlands: Application to five wetland sites, sensitivity to model parameters, and climate. *Global Biogeochemical Cycles,* 14**,** 745-765.

Walter, B. P., M. Heimann & E. Matthews (2001) Modeling modern methane emissions from natural wetlands 1. Model description and results. *Journal of Geophysical Research-Atmospheres,* 106**,** 34189-34206.

Wania, R., I. Ross & I. C. Prentice (2009a) Integrating peatlands and permafrost into a dynamic global vegetation model: 1. Evaluation and sensitivity of physical land surface processes. *Global Biogeochemical Cycles,* 23**,** GB3014, doi: 10.1029/2008GB003412.

--- (2009b) Integrating peatlands and permafrost into a dynamic global vegetation model: 2. Evaluation and sensitivity of vegetation and carbon cycle processes. *Global Biogeochemical Cycles,* 23**,** GB3015, doi: 10.1029/2008GB003413.

--- (2010) Implementation and evaluation of a new methane model within a dynamic global vegetation model: LPJ-WHyMe v1.3.1. *Geoscientific Model Development,* 3**,** 565-584.

WCMC: UNEP World Conservation Monitoring Centre, 1993. Digital Wetlands Data set. Cambridge, UK. Data obtained from WCMC in 1999.

Wramneby, A., B. Smith, S. Zaehle & M. T. Sykes (2008) Parameter uncertainties in the modelling of vegetation dynamics—Effects on tree community structure and ecosystem functioning in European forest biomes. *Ecological Modelling,* 216**,** 277-290.

Zaehle, S., S. Sitch, B. Smith & F. Hatterman (2005) Effects of parameter uncertainties on the modeling of terrestrial biosphere dynamics. *Global Biogeochemical Cycles,* 19.

Zhuang, Q., J. M. Melillo, D. W. Kicklighter, R. G. Prinn, A. D. McGuire, P. A. Steudler, B. S. Felzer & S. Hu (2004) Methane fluxes between terrestrial ecosystems and the atmosphere at northern high latitudes during the past century: A retrospective analysis with a process-based biogeochemistry model. *Global Biogeochemical Cycles,* 18.

Zhuang, Q. L., J. M. Melillo, M. C. Sarofim, D. W. Kicklighter, A. D. McGuire, B. S. Felzer, A. Sokolov, R. G. Prinn, P. A. Steudler & S. M. Hu (2006) CO2 and CH4 exchanges between land ecosystems and the atmosphere in northern high latitudes over the 21st century. *Geophysical Research Letters,* 33. Zobler, L., A world soil file for global climate modeling, NASA Tech. Memo. 87802, 32 pp., 1986.

Zobler, L., A world soil file for global climate modeling, NASA Tech. Memo. 87802, 32 pp., 1986.

Institutionen för naturgeografi och ekosystemvetenskap, Lunds Universitet.

Student examensarbete (Seminarieuppsatser). Uppsatserna finns tillgängliga på institutionens geobibliotek, Sölvegatan 12, 223 62 LUND. Serien startade 1985. Hela listan och själva uppsatserna är även tillgängliga på LUP student papers (www.nateko.lu.se/masterthesis) och via Geobiblioteket (www.geobib.lu.se)

The student thesis reports are available at the Geo-Library, Department of Physical Geography and Ecosystem Science, University of Lund, Sölvegatan 12, S-223 62 Lund, Sweden. Report series started 1985. The complete list and electronic versions are also electronic available at the LUP student papers (www.nateko.lu.se/masterthesis) and through the Geo-library (www.geobib.lu.se)

266 Iurii Shendryk (2013) Integration of LiDAR data and satellite imagery for biomass estimation in conifer-dominated forest
267 Kristian Morin (2013) Mapping moth induced birch forest damage in northern Sweden, with MODIS satellite data
268 Ylva Persson (2013) Refining fuel loads in LPJ-GUESS-SPITFIRE for wet-dry areas - with an emphasis on Kruger National Park in South Africa
269 Md. Ahsan Mozaffar (2013) Biogenic volatile organic compound emissions from Willow trees
270 Lingrui Qi (2013) Urban land expansion model based on SLEUTH, a case study in Dongguan City, China
271 Hasan Mohammed Hameed (2013) Water harvesting in Erbil Governorate, Kurdistan region, Iraq - Detection of suitable sites by using Geographic Information System and Remote Sensing
272 Fredrik Alström (2013) Effekter av en havsnivåhöjning kring Falsterbohalvön.
273 Lovisa Dahlquist (2013) Miljöeffekter av jordbruksinvesteringar i Etiopien
274 Sebastian Andersson Hylander (2013) Ekosystemtjänster i svenska agroforestrysystem
275 Vlad Pirvulescu (2013) Application of the eddy-covariance method under the canopy at a boreal forest site in central Sweden
276 Malin Broberg (2013) Emissions of biogenic volatile organic compounds in a Salix biofuel plantation – field study in Grästorp (Sweden)
277 Linn Renström (2013) Flygbildsbaserad förändringsstudie inom skyddszoner längs vattendrag
278 Josefin Methi Sundell (2013) Skötseleffekter av miljöersättningen för natur- och kulturmiljöer i odlingslandskapets småbiotoper
279 Kristín Agustsdottír (2013) Fishing from Space: Mackerel fishing in Icelandic waters and correlation with satellite variables
280 Cristián Escobar Avaria (2013) Simulating current regional pattern and composition of Chilean native forests using a dynamic ecosystem model
281 Martin Nilsson (2013) Comparison of MODIS-Algorithms for Estimating Gross Primary Production from Satellite Data in semi-arid Africa
282 Victor Strevens Bolmgren (2013) The Road to Happiness – A Spatial Study of Accessibility and Well-Being in Hambantota, Sri Lanka
283 Amelie Lindgren (2013) Spatiotemporal variations of net methane emissions and its causes across an ombrotrophic peatland - A site study from Southern Sweden
284 Elisabeth Vogel (2013) The temporal and spatial variability of soil respiration in boreal forests - A case study of Norunda forest, Central Sweden

285 Cansu Karsili (2013) Calculation of past and present water availability in the Mediterranean region and future estimates according to the Thornthwaite water-balance model
286 Elise Palm (2013) Finding a method for simplified biomass measurements on Sahelian grasslands
287 Manon Marcon (2013) Analysis of biodiversity spatial patterns across multiple taxa, in Sweden
288 Emma Li Johansson (2013) A multi-scale analysis of biofuel-related land acquisitions in Tanzania - with focus on Sweden as an investor
289 Dipa Paul Chowdhury (2013) Centennial and Millennial climate-carbon cycle feedback analysis for future anthropogenic climate change
290 Zhiyong Qi (2013) Geovisualization using HTML5 - A case study to improve animations of historical geographic data
291 Boyi Jiang (2013) GIS-based time series study of soil erosion risk using the Revised Universal Soil Loss Equation (RUSLE) model in a micro-catchment on Mount Elgon, Uganda
292 Sabina Berntsson & Josefin Winberg (2013) The influence of water availability on land cover and tree functionality in a small-holder farming system. A minor field study in Trans Nzoia County, NW Kenya
293 Camilla Blixt (2013) Vattenkvalitet - En fältstudie av skånska Säbybäcken
294 Mattias Spångmyr (2014) Development of an Open-Source Mobile Application for Emergency Data Collection
295 Hammad Javid (2013) Snowmelt and Runoff Assessment of Talas River Basin Using Remote Sensing Approach
296 Kirstine Skov (2014) Spatiotemporal variability in methane emission from an Arctic fen over a growing season – dynamics and driving factors
297 Sandra Persson (2014) Estimating leaf area index from satellite data in deciduous forests of southern Sweden
298 Ludvig Forslund (2014) Using digital repeat photography for monitoring the regrowth of a clear-cut area
299 Julia Jacobsson (2014) The Suitability of Using Landsat TM-5 Images for Estimating Chromophoric Dissolved Organic Matter in Subarctic Lakes
300 Johan Westin (2014) Remote sensing of deforestation along the trans-Amazonian highway
301 Sean Demet (2014) Modeling the evolution of wildfire: an analysis of short term wildfire events and their relationship to meteorological variables
302 Madelene Holmblad (2014). How does urban discharge affect a lake in a recreational area in central Sweden? – A comparison of metals in the sediments of three similar lakes
303 Sohidul Islam (2014) The effect of the freshwater-sea transition on short-term dissolved organic carbon bio-reactivity: the case of Baltic Sea river mouths
304 Mozafar Veysipanah (2014) Polynomial trends of vegetation phenology in Sahelian to equatorial Africa using remotely sensed time series from 1983 to 2005
305 Natalia Kelbus (2014) Is there new particle formation in the marine boundary layer of the North Sea?
306 Zhanzhang Cai (2014) Modelling methane emissions from Arctic tundra wetlands: effects of fractional wetland maps